



# 1 Spatial and temporal distribution of fine aerosol acidity in the 2 Eastern Mediterranean

3

4 Anna Maria Neroladaki<sup>1,2</sup>, Maria Tsagkaraki<sup>1</sup>, Kyriaki Papoutsidaki<sup>1</sup>, Kalliopi Tavernarakis<sup>1</sup>, Filothei  
5 Boufidou<sup>3</sup>, Pavlos Zarmpas<sup>1</sup>, Irini Tsiodra<sup>4</sup>, Eleni Liakakou<sup>4</sup>, Aikaterini Bougiatioti<sup>4</sup>, Giorgos  
6 Kouvarakis<sup>1</sup>, Nikos Kalivitis<sup>1</sup>, Christos Kaltsonoudis<sup>2</sup>, Athanasios Karagioras<sup>5</sup>, Dimitris Balis<sup>6</sup>,  
7 Konstantinos Mihailidis<sup>6</sup>, Konstantinos Kourtidis<sup>5</sup>, Stelios Myriokefalitakis<sup>4</sup>, Nikos Hatzianastassiou<sup>7</sup>,  
8 Spyros N. Pandis<sup>2</sup>, Athanasios Nenes<sup>2,8</sup>, Nikolaos Mihalopoulos<sup>1,3</sup> and Maria Kanakidou<sup>1,2,7</sup>

9

10 <sup>1</sup>Environmental Chemical Processes Laboratory (ECPL), Department of Chemistry, University of Crete, 70013  
11 Heraklion, Greece

12 <sup>2</sup>Center for Studies of Air Quality and Climate Change, Institute for Chemical Engineering Sciences, Foundation  
13 for Research and Technology Hellas, 26504 Patras, Greece

14 <sup>3</sup>Institute of Environmental Physics, University of Bremen, 28359 Bremen, Germany

15 <sup>4</sup>Institute for Environmental Research and Sustainable Development, National Observatory of Athens, 15236  
16 Palea Penteli, Greece

17 <sup>5</sup>Department of Environmental Engineering, Democritus University of Thrace, 67100 Xanthi, Greece

18 <sup>6</sup>Laboratory of Atmospheric Physics, Aristotle University of Thessaloniki, 54634 Thessaloniki, Greece

19 <sup>7</sup>Laboratory of Meteorology, Department of Physics, University of Ioannina, 45110 Ioannina, Greece

20 <sup>8</sup>Laboratory of Atmospheric Processes and their Impacts, School of Architecture, Civil and Environmental  
21 Engineering, Ecole Polytechnique Fédérale de Lausanne, 1015, Lausanne, Switzerland

22

23 *Correspondence to:* Maria Kanakidou (mariak@uoc.gr)

24 **Abstract.** Aerosol acidity (pH) affects aerosol composition and properties, and therefore climate, human health  
25 and ecosystems. Fine aerosol acidity and its seasonal variation at 6 sites (Finokalia, Patras, Thissio, Ioannina,  
26 Thessaloniki, and Xanthi) in Greece were investigated during 2019-2020. The thermodynamic model  
27 ISORROPIA-lite was used to calculate aerosol water and acidity based on measurements of the chemical  
28 composition of PM<sub>2.5</sub> and available gas-phase concentrations of HNO<sub>3</sub>, NH<sub>3</sub>, and HCl. During winter the fine  
29 aerosols were acidic to moderately acidic throughout Greece with an overall mean aerosol pH of 3.57±0.44 in  
30 urban areas and 3.05±0.50 in remote locations. The highest aerosol pH (4.08±0.42) in January 2020 was found in  
31 Ioannina due to, among others, high K<sup>+</sup> levels from biomass burning emissions. Aerosols in Xanthi were the most  
32 acidic due to high sulfate levels. Similar seasonal profiles of aerosol pH were observed at all sites studied with  
33 different factors contributing to this seasonality. During the summer PM<sub>2.5</sub> at Thissio, Ioannina and Finokalia was  
34 acidic with a mean aerosol pH across all three sites of 1.76±0.40. During this season, sulfates were the driver of  
35 the higher acidity conditions at Thissio and Finokalia, with other factors such as the semivolatiles and temperature  
36 contributing to a lesser extent. At Ioannina, temperature along with the total ammonia and nitrate were the main  
37 contributors to the seasonal difference of the aerosol pH, while some of the nonvolatile species also contributed.  
38 In most cases, the importance of organics for aerosol pH was small.

39

40

## 41 1 Introduction



42 The aerosol pH is one of the most important chemical properties of aerosols. It controls the rates of several  
43 reactions in the particulate phase (e.g., sulfate and oligomer formation reactions in the particulate phase) and  
44 governs the gas-particle partitioning of semivolatile gases such as ammonia ( $\text{NH}_3$ ), nitric acid ( $\text{HNO}_3$ ) and  
45 hydrochloric acid ( $\text{HCl}$ ), and some organic acids with low molecular weight (formic, oxalic, acetic etc.) and bases  
46 (e.g. amines). Several studies have thoroughly discussed the importance of the gas phase  $\text{NH}_3$  and  $\text{HNO}_3$  and their  
47 effect on the particulate matter as well as their relationship with aerosol pH and water (Pye et al., 2020; Nenes et  
48 al., 2020; Guo et al., 2018, 2016, 2017b).  $\text{NH}_3$  from anthropogenic and biogenic emissions is the most important  
49 gaseous base in the atmosphere, while  $\text{HNO}_3$  is an acid produced by the oxidation of  $\text{NO}_x$  mainly emitted by  
50 combustion sources (Seinfeld and Pandis, 2006).  $\text{HNO}_3$ , because of its strong acidity and solubility, partitions  
51 more in the gas phase than in the particle phase (as nitrate) at lower aerosol pH (usually below 1.5 to 2) (Weber  
52 et al., 2016), while  $\text{NH}_3$  remains in the gas phase at higher pH. These processes have serious implications for the  
53 wet and dry deposition of these semivolatile pollutants on ecosystems, their lifetime, climate and human health  
54 (Pye et al., 2020).

55 Metal cations, including those that originate from dust and sea salt, are nonvolatile at atmospheric  
56 temperatures. These constituents seriously affect the aerosol pH together with parameters such as the  
57 meteorological conditions (i.e. temperature and relative humidity). These parameters and the availability of  
58 sulfuric acid (that partitions almost exclusively to the particulate phase) are mostly responsible for the wide range  
59 of the pH of atmospheric particles (Pye et al., 2020).

60 Aerosol pH affects the uptake of sulfur dioxide ( $\text{SO}_2$ ) into the aerosol aqueous phase and its oxidation to sulfate  
61 (Seinfeld and Pandis, 2006). This is important for climate, as sulfate is one of the main scattering components of  
62 atmospheric aerosols with a cooling effect on climate. Acid catalyzed reactions lead to the formation of brown  
63 carbon that is an important contributor to absorbing aerosol (Zhang et al., 2020). Atmospheric acidity affects  
64 aerosol toxicity, controlling the solubilization of toxic forms of transition and heavy metals, such as copper and  
65 iron (Fang et al., 2017) with adverse impacts on human health (Vierke et al., 2013). Furthermore, acidity increases  
66 the solubility and thus the bioavailability of iron, phosphorus and trace metals that are deposited on ecosystems  
67 (Pye et al., 2020). This is of a great importance in oligotrophic areas, such as the East Mediterranean Sea, a marine  
68 desert, characterized by extremely low biological productivity, due to the limited availability of nutrients like  
69 phosphate (Powley et al., 2017). The area is frequently influenced by dust outbreaks from the Saharan desert,  
70 which contain several minerals and metals primarily in insoluble forms. The conversion of insoluble to soluble  
71 bioavailable form of a given nutrient is favored under acidic conditions (Kanakidou et al., 2018; Nenes et al.,  
72 2011). The solubility of iron and thus its bioavailability to ecosystems, is also controlled by acidity, as it is  
73 enhanced in the presence of acidic species. Theodosi et al. (2008) found that in the Eastern Mediterranean the iron  
74 solubility ranged from 28% for polluted rainwater (pH 4-5) to 0.5% for Sahara dust episodes (pH=8).

75 Although the acidity of atmospheric particles plays such a critical role in all of the atmospheric processes  
76 mentioned above, there is no direct method for its accurate measurement due to the miniscule sample mass and  
77 liquid volume (Pye et al., 2020). Thus, several indirect methods have been developed, which estimate aerosol  
78 acidity (Pye et al., 2020). One of the best available methods is the aerosol pH prediction using atmospheric aerosol  
79 thermodynamic models in combination with measurements of aerosol composition and gas-phase nitric acid,  
80 ammonia and hydrochloric acid concentrations. Models such as ISORROPIA II (Fountoukis and Nenes, 2007),



81 MOSAIC (Zaveri et al., 2008), E-AIM; (Clegg et al., 2001; Wexler and Clegg, 2002), etc. can be used to this  
82 purpose.

83 Aerosols' acidity covers a wide range and aerosol pH can be as high as about 7 pH units (sea salt), and as low  
84 as -1 and sometimes even -2 pH units, depending on the composition of the aerosol and the meteorological  
85 conditions in a given area (Pye et al., 2020). Negative values appear when sulfates are the dominant constituent  
86 of particulate matter, while the aerosol pH rarely rises above neutral levels. Globally fine atmospheric particles  
87 ( $PM_{2.5}$ ) have been found to have a bimodal acidity pattern with one population of smaller particles having an  
88 average pH between 1 and 3 pH units, and another of larger particles with a mean pH close to 4 and 5 units, which  
89 is due to the influence of dust, sea spray and biomass burning (Sindosi et al., 2012; Pye et al., 2020).

90 Several studies have investigated the levels of the acidity of fine particles and their major drivers at specific  
91 sites. For instance, studies in Beijing and close-by locations indicate a mean wintertime  $PM_{2.5}$  pH of 4.2 to 4.9  
92 units (Liu et al., 2017; Guo et al., 2017a; Shi et al., 2017; Ding et al., 2019). Pye et al. (2020) summarized and  
93 investigated the fine aerosol pH in several regions globally and reported that overall aerosol pH is consistently  
94 acidic and looking into the seasonality, during wintertime where low temperature and high relative humidity  
95 occur, aerosol pH was higher compared to summertime following the temperature and the availability of liquid  
96 water content. Tao and Murphy (2019) reported that in winter the pH of fine aerosols was around 3 units at 6 sites  
97 in Canada and was strongly influenced by temperature, relative humidity and aerosol chemical composition.  
98 Kakavas et al. (2021) simulated the aerosol acidity and its variation with size and altitude over Europe during  
99 summer and found the ground level mean aerosol pH across the domain to be 2.05 for  $PM_{10}$ , 2.65 for  $PM_{1-2.5}$ , 3.2  
100 for  $PM_{2.5-5.5}$  and 3.35 for  $PM_{5-10}$ . The lowest aerosol pH was reported in the Mediterranean and especially in the  
101 eastern Mediterranean where high sulfate and nitrate levels were predicted. This study suggests that Eastern  
102 Mediterranean can be an especially interesting region for aerosol pH studies.

103 There have been only limited estimations of aerosol acidity in the eastern Mediterranean. The  $PM_{2.5}$  pH in 6  
104 cities in the eastern Po Valley in Italy (Masiol et al., 2020) was found to range from 1.5 to 4.5 with summer  
105 minima and winter maxima and mean pH values across all sites of  $2.2 \pm 0.3$  and  $3.9 \pm 0.3$ , respectively. These  
106 levels of fine aerosol acidity were mainly driven by secondary sulfate, fossil fuel combustion, secondary nitrate  
107 and biomass burning. An earlier study in the same area (Squizzato et al., 2013) investigated seasonally the aerosol  
108 pH and found that in spring the aerosol pH was higher compared to summer (average aerosol pH across the sites;  
109 spring 3.6 pH units, summer 2.3, autumn 3, winter 3.6) as a result of desert dust aerosol originating from the  
110 Sahara desert. Again in Po Valley, a multiyear (25 years) trend of fog water pH and aerosol pH was estimated  
111 (Paglione et al., 2021) and an opposite trend between them was found; there was an increase in the fog water pH  
112 and a decrease in fine aerosol acidity. In fact, there was a decrease of 0.5-1.5 pH units in the aerosol pH, trend  
113 that was driven by the contemporary decrease of the corresponding air pollutants due to environmental policies in  
114 combination with the changing meteorology (temperature and relative humidity levels). Lastly, the submicron  
115 aerosol pH was estimated in a study conducted at the Finokalia atmospheric observation station in Greece  
116 (Bougiatioti et al., 2016) and was found to be highly acidic ranging from 0.5 to 2.8 pH units with daytime  
117 minimum and nighttime maximum values due to low aerosol water content and high temperatures during the day.  
118 They also pointed out the influence of biomass burning which increased the aerosol pH values highlighting the  
119 impact of nonvolatile cations, mainly potassium from biomass burning together with ammonia and nitrate emitted



120 from wood burning. Despite these studies, the spatial distribution of aerosol acidity based on atmospheric  
121 composition observations is not well understood.

122 The present study aims to provide a spatial and seasonal picture of the acidity of fine ( $PM_{2.5}$ ) atmospheric  
123 aerosol over Greece in the eastern Mediterranean based on observations of atmospheric composition. For this, the  
124 ISORROPIA-lite thermodynamic equilibrium model (Kakavas et al., 2022) is used together with observations of  
125 the chemical composition of the fine aerosol from 6 sites over Greece and with gas phase  $NH_3$  and  $HNO_3$  data,  
126 where available. The water and pH of the fine aerosol are estimated during summer 2019 and winter 2019-2020.  
127 The factors controlling the seasonality of aerosol pH are examined and the effect of particulate organic matter on  
128 aerosol pH predictions is also investigated.

## 129 2 Measurements and Methodology

### 130 2.1 Measurement sites

131 Measurements of the chemical composition of  $PM_{2.5}$  were performed at 6 sites across Greece (Fig. 1) (Finokalia,  
132 Thissio, Patra, Ioannina, Xanthi and Thessaloniki, Table S1). The corresponding summer and winter field  
133 campaigns were conducted within the PANACEA (PANhellenic infrastructure for Atmospheric Composition and  
134 climatE chAnge) project during the summer of 2019 and the winter of 2019-2020.

135 The Finokalia atmospheric observatory of the University of Crete in Crete, Greece (FKL, 35.33° N, 25.67° E;  
136 250 m a.s.l.) is a remote regional background site in the northeast coast of the island of Crete (south Greece). The  
137 site is not subject to any major anthropogenic influence and it is considered as a representative background site  
138 for the entire eastern Mediterranean. During the warm months of the year (April to September, dry season) the  
139 station mainly receives air masses from the N/NW (originating from the Central and Eastern Europe and the  
140 Balkans), while between October and April (wet season) air masses coming from the South lead to Saharan dust  
141 events (Mihalopoulos et al., 1997).

142 The Thissio Air Monitoring station (THI, 37.97° N, 23.72° E, 105 m a.s.l.) of the National Observatory of  
143 Athens, Greece is located approximately 50 m above the mean city level near the historical city center. The station  
144 is an urban background site due to its distance from traffic and industrial emission sources and receives air  
145 pollutants from various urban and regional sources.

146 The Patras site is located at the Institute of Chemical Engineering Sciences (ICE-HT) of FORTH (Foundation  
147 for Research and Technology, Hellas), which is in Platani (PTR, 38.30° N, 21.81° E, 100 m a.s.l.) 8 km from the  
148 city center. It is an urban background site. Local sources include transportation, biomass burning (both residential  
149 and agricultural) and shipping emissions, while long-range transport is the dominant  $PM_{2.5}$  source during most  
150 periods (Pikridas et al., 2013).

151 The Xanthi station is operated by the Laboratory of Atmospheric Pollution and Pollution Control Engineering  
152 of Atmospheric Pollutants of the Department of Environmental Engineering. The station is located in the  
153 Kimmeria DUTH campus (XAN, 41.15° N, 24.92° E; 75 m a.s.l.) almost 2 km from the city of Xanthi in  
154 northeastern Greece. The station is a rural site and the edge of a slope facing to the south, 20 km away from the  
155 seashore. The Rodopi Mountain Range is located to the north of the station. The prevailing winds that reach the  
156 site in winter are fairly stable SW/S/SE during the day, but they change to N/NW at night; the location of the site



157 between mountains and a valley creates a closed circulation cell of valley/land breezes (Kastelis and Kourtidis,  
158 2016).

159 The Thessaloniki station at the north of Greece is at the Laboratory of Atmospheric Physics (LAP) which is  
160 located at the School of Sciences of the Aristotle University of Thessaloniki (LAP, 40.63°N, 22.95°E; 50m a.s.l.).  
161 Thessaloniki is a coastal city at Thermaikos Gulf and is the second largest city in Greece. The site experiences air  
162 pollution episodes due to the meteorological conditions over northern Greece; with high pressure, anticyclonic  
163 systems and sunny weather in summer, while colder temperatures near the surface and snow occur in winter  
164 (Flocas et al., 2009). It is considered as a representative urban station.

165 Ioannina (IOA, 39.653195°N, 20.854208°E) is located in Epirus Region in northwestern Greece, which is  
166 separated from the eastern part of the country mainland by the Pindus mountain range (orientated from NW to SE  
167 and exceeding 2000 m in height). The sampling station was located at a kindergarten yard, 1.5 km from Ioannina's  
168 city center. Ioannina is located on a plateau of about 500 m altitude and is surrounded by mountains. The city is  
169 next to the Pamvotis lake and is characterized by frequent fog events in winter, due to increased relative humidity,  
170 weak winds and basin-like attributes and winter biomass burning events (Kaskaoutis et al., 2020).

## 171 2.2 Measurements

172 The PANACEA campaigns took place at the 6 sites discussed above during the summer of 2019 and the winter  
173 of 2019-2020. Atmospheric particles were collected daily on quartz-fiber filters using high-volume or low-volume  
174 aerosol samplers depending on the site. A Sunset Organic Carbon (OC) /Elemental Carbon (EC) analyzer was  
175 used to determine the concentrations of OC and EC, while the inorganic cations:  $\text{NH}_4^+$ ,  $\text{K}^+$ ,  $\text{Ca}^{2+}$ ,  $\text{Mg}^{2+}$ ,  $\text{Na}^+$  and  
176 anions:  $\text{SO}_4^{2-}$ ,  $\text{Cl}^-$  and  $\text{NO}_3^-$  were determined using ion chromatography. Details on the methods of the  $\text{PM}_{2.5}$  filter  
177 analysis during the PANACEA winter and summer campaign can be found in (Kaskaoutis et al., 2022). In situ-  
178 measurements of temperature and relative humidity were also available for the period of the campaigns (Fig S1  
179 and S2).

180 For the campaign period there were not available gas phase concentrations ( $\text{NH}_3$ ,  $\text{HNO}_3$ ) measurements at any  
181 of the 6 sampling sites except PTR ( $\text{NH}_3$ ). Thus, for  $\text{NH}_3$ , satellite data were used for the remaining sites (except  
182 IOA during the winter campaign period). For  $\text{HNO}_3$ , past in situ measurements were used at FKL and for the other  
183 sites (THI, PTR, IOA, LAP, XAN) past in situ measurements conducted at THI were used.

184 In more detail, the Patras site as mentioned above, was the only site with available gas-phase  $\text{NH}_3$   
185 measurements for the studied periods during the 2019-2020 winter campaign, with mean ammonia concentration  
186 of  $2.54 \pm 0.90 \mu\text{g}/\text{m}^3$ . At IOA during the wintertime period of the study, neither in situ observations nor satellite  
187 data were available and thus  $\text{NH}_3$  observations at PTR were used for IOA. Therefore, the mean ammonia  
188 concentration value from PTR dataset was also used for the IOA wintertime simulations.

189 For the other sites (FKL and THI during winter and summer, and LAP and XAN during winter)  $\text{NH}_3$  data  
190 (level 2 data, version 1.6.3) were used from the Cross-track Infrared Sounder (CrIS) instrument which is deployed  
191 on board the Suomi National Polar-orbiting Partnership (SNPP) platform (into an orbit with an altitude of 824 km  
192 above the Earth surface) (Shephard and Cady-Pereira, 2015). Ammonia values over these sites were obtained  
193 from the CrIS Fast Physical Retrieval (CFPR) product, which provides  $\text{NH}_3$  concentration data for a total of 15  
194 vertical levels, with the value closest to the ground being taken as the near-surface concentration. From the



195 available CrIS near-surface  $\text{NH}_3$  concentrations within a 50-km diameter area around each site, the value within  
196 the pixel at the closest distance to the site is retained (Shephard et al., 2020; Shephard and Cady-Pereira, 2015).  
197 The wintertime near-surface  $\text{NH}_3$  concentrations as derived from CrIS for FKL, THI, XAN and LAP are shown  
198 in Fig. 2. For summer at FKL and THI, mean values of summertime near-surface  $\text{NH}_3$  (from 13/08/2019 to  
199 19/08/2019 for FKL and from 13/08/2019 to 31/08/2019 for THI)  $1.24 \pm 0.61 \mu\text{g}/\text{m}^3$  and  $1.32 \pm 1.53 \mu\text{g}/\text{m}^3$   
200 respectively, were used due to the scarcity of summertime data from CrIS in 2019.

201 For IOA during summer, a mean  $\text{NH}_3$  concentration of  $1.04 \mu\text{g}/\text{m}^3$  was used as derived from the Atmospheric  
202 Infrared Sounder (AIRS) aboard NASA's Aqua satellite (Level 3 data) operating from September 2002 to August  
203 2016 (Warner et al., 2016) (the mean summertime 2002-2016 concentration was used).

204 For  $\text{HNO}_3$  and  $\text{HCl}$  gas-phase concentration measurements, samples were collected only at Finokalia (2015 -  
205 2016) using glass fiber filters coated with  $\text{Na}_2\text{CO}_3$  and were analyzed by ion chromatography. The median of  
206 these gas-phase measurements of  $\text{HNO}_3$  and  $\text{HCl}$  were used here ( $0.63 \mu\text{g}/\text{m}^3$  and  $0.98 \mu\text{g}/\text{m}^3$  for winter and  $0.95$   
207  $\mu\text{g}/\text{m}^3$  and  $1.34 \mu\text{g}/\text{m}^3$  for summer, respectively). For all other sites, gas-phase measurements of  $\text{HNO}_3$  conducted  
208 at Thissio from 12/2014 to 3/2016 (Liakakou et al., 2022) were used here as mean values ( $0.53 \pm 0.12 \mu\text{g}/\text{m}^3$  for  
209 winter and  $0.91 \pm 0.29 \mu\text{g}/\text{m}^3$  for summer).

210 Since the  $\text{NH}_3$  in situ observations at PTR did not coincide with any CrIS or AIRS data, a comparison between  
211 in situ and satellite data was not possible. The sensitivity of our pH estimates to these assumed  $\text{NH}_3$  and  $\text{HNO}_3$   
212 concentrations will be examined in a subsequent section (see section 3.4).

213

### 214 2.3 pH Estimation

215 The pH of the fine aerosol at the 6 studied sites, was calculated using ISORROPIA-lite thermodynamic model  
216 (Kakavas et al., 2022), which is an extension of the ISORROPIA-II model (Fountoukis and Nenes, 2007).  
217 ISORROPIA-lite treats the same system of aerosols as ISORROPIA-II ( $\text{Ca}^{2+}$ ,  $\text{K}^+$ ,  $\text{Mg}^{2+}$ ,  $\text{SO}_4^{2-}$ ,  $\text{Na}^+$ ,  $\text{NH}_4^+$ ,  $\text{NO}_3^-$ ,  
218  $\text{Cl}^-$ ,  $\text{H}_2\text{O}$  and their equilibrium with the gas phase  $\text{HNO}_3$ ,  $\text{NH}_3$ ,  $\text{HCl}$  and  $\text{H}_2\text{O}$ ) with the addition of the organic  
219 aerosol and considering only the deliquescent aerosol at all RH values. The addition of organic matter in the  
220 thermodynamic equilibrium aerosol system, results in more aerosol water which favors the partitioning of  
221 semivolatile inorganic species into the aerosol phase in order to satisfy the equilibrium (Kakavas et al., 2022).  
222 The particle water ( $W_{\text{org}}$ ) associated with the organic aerosol is implemented in the model using the hygroscopicity  
223 parameter ( $\kappa_{\text{org}}$ ). The total aerosol water content, i.e. the water associated with the inorganic and organic parts of  
224 the aerosol, is the sum of the inorganic and organic water and it is used in the thermodynamic calculations. The  
225 aerosol pH is then calculated by:

$$227 \quad \text{pH} = -\log_{10} \frac{1000 \gamma_{\text{H}^+} [\text{H}_{\text{air}}^+]}{[W_{\text{inorg}}] + [W_{\text{org}}]} \quad (1)$$

228 where  $\gamma_{\text{H}^+}$  is the activity coefficient of the hydronium ion ( $\text{H}^+$ ) here assumed unity,  $\text{H}_{\text{air}}^+$  is the equilibrium particle  
229 hydronium ion concentration per volume air ( $\mu\text{g}/\text{m}^3$ ),  $W_{\text{inorg}}$  and  $W_{\text{org}}$  is the water associated with the inorganic  
230 and organic part of the aerosol, respectively (both in  $\mu\text{g}/\text{m}^3$ ). Thus, the aerosol pH was calculated including the  
231 contribution of the organic aerosol hence the aerosol water associated with both inorganic and organic species.



To calculate the aerosol water content associated with the organic species, the total organic aerosol concentration (OA) derived from the OC measurements at each site is used together with an OA/OC ratio of 1.8 for all sites. This average ratio is consistent with the results of measurements conducted at the same sites (Florou et al., 2017; Hildebrandt et al., 2011; Kaskaoutis et al., 2020, 2022; Kostenidou et al., 2015; Pikridas et al., 2013; Stavroulas et al., 2019; Tsiflikiotou et al., 2019). The hygroscopicity parameter was set to  $\kappa_{\text{org}} = 0.16$  for Finokalia as suggested in studies for this site (Bougiatioti et al., 2009; Kalkavouras et al., 2019), and  $\kappa_{\text{org}} = 0.12$  for the other sites (Psichoudaki et al., 2018).

### 3 Results and Discussion

#### 3.1 Aerosol Composition

The chemical composition and mass concentration of the major species in  $\text{PM}_{2.5}$  measured during the PANACEA campaigns are summarized in Table 1. The dominant  $\text{PM}_{2.5}$  component was OA at all sites except FKL, where sulfate dominated both in winter and summer. This is typical for remote background sites (Lemou et al., 2020; Sciare et al., 2008). Higher sulfate levels were present in FKL during summer due to high temperatures and photochemistry, followed by organics (typically consisting 20-30% of the  $\text{PM}_{2.5}$  mass, Pikridas et al., 2010; Putaud et al., 2004). The highest levels of OA were observed at Ioannina (IOA) during winter. OA represented more than 60% of the  $\text{PM}_{2.5}$  and was mainly due to residential wood burning emissions while the meteorology and topography of the area facilitated the accumulation of all pollutants (Kaskaoutis et al., 2022). Much lower levels of OA and  $\text{PM}_{2.5}$  mainly of regional origin, were measured at IOA in the summer (Kaskaoutis et al., 2022). At the three sites where measurements were available in the summer (IOA, FKL, THI), sulfate was a major component of the  $\text{PM}_{2.5}$  despite their different characteristics. Inorganic  $\text{PM}_{2.5}$  across all sites in winter was dominated by sulfate except IOA where, interestingly,  $\text{NO}_3^-$  was the dominant inorganic  $\text{PM}_{2.5}$  component due to possible high  $\text{NO}_x$  emissions, or  $\text{NO}_x$  accumulation in the boundary layer due to low inversion heights and decreased horizontal circulation, the latter due to surrounding mountains. The  $\text{K}^+$  levels in IOA were also elevated indicating the influence of biomass burning in the area (Kaskaoutis et al., 2022).

#### 3.2 Aerosol pH across Greece

##### 3.2.1 Winter

The distributions of estimated pH of  $\text{PM}_{2.5}$  as derived from the ISORROPIA-lite model for the 6 studied sites during winter (January 2020) is shown in Fig. 3a.

In January the aerosols at THI were slightly acidic with a wide range of pH values (2.17 to 4.17), reflecting the variation of the  $\text{PM}_{2.5}$  composition and meteorology. The mean pH was  $3.30 \pm 0.48$  (median 3.34). Days with highly acidic aerosol, i.e. pH below 2.5, were associated with elevated sulfate levels and northerly winds. At FKL the mean aerosol pH was  $3.25 \pm 0.37$  and ranged from 2.73 to 3.89 (median 3.30). The elevated pH coincided with high concentrations of nonvolatile cations (NVC) and  $\text{NH}_3$  and the lower pH values (less than 2.8) occurred during periods with high levels of sulfates. In the northern part of Greece, at XAN the pH range covered 2.24 units with a mean value of  $2.81 \pm 0.53$  (median 2.69). The shift between acidic and moderately acidic conditions



was associated with changes mainly in  $\text{NH}_3$  and sulfate levels. Days when pH reached almost 4, were characterized by high potassium in combination with high OA and EC levels and low sulfates suggesting significant influence of biomass burning. At LAP the pH of  $\text{PM}_{2.5}$  ranged from 2.72 to 3.41, with a mean value of  $3.01 \pm 0.31$ . Please note that only 4 days of  $\text{PM}_{2.5}$  measurements were available in LAP during January 2020. The fine aerosol in IOA had the lowest overall acidity with a mean value of  $4.08 \pm 0.42$  units and a range between 3.55 and 5.14 units. These levels of acidity are a consequence of the intense biomass burning during this winter campaign at IOA (Kaskaoutis et al., 2022). Elevated  $\text{K}^+$  levels were observed, due almost entirely to wood burning for heating. Comparing IOA with the other sites in January, there is a statistically significant difference in aerosol acidity levels due to higher  $\text{Ca}^{2+}$ ,  $\text{K}^+$  and  $\text{NH}_3$  combined with lower temperature, despite the high sulfates levels in the area (Table 1). At PTR aerosol pH ranged from 2.82 to 4.44 units with a mean value of  $3.70 \pm 0.45$ . NVCs ( $\text{Ca}^{2+}$ ,  $\text{K}^+$ ,  $\text{Mg}^{2+}$  and  $\text{Na}^+$ ),  $\text{NH}_3$  and sulfates drove the variability of the aerosol pH most of the days. Aerosols at LAP and XAN exhibited the highest acidity (lowest pH levels) among all studied sites, while IOA and PTR exhibited the highest aerosol pH levels (Fig. 3a). Remarkably, aerosol acidity at the urban background site (THI) was similar to that at the coastal background site (FKL). On the other hand, the suburban site (PTR) had higher aerosol pH mainly due to the likely higher  $\text{NH}_3$  levels at PTR than THI and FKL (Table 1), considering though the different ways  $\text{NH}_3$  was measured for these sites. Considering the two remote rural and coastal areas (XAN and FKL), their fine aerosol pH differed by about half a pH unit due to increased  $\text{Na}^+$ ,  $\text{Mg}^{2+}$  and relative humidity levels at FKL together with slightly higher sulfate concentrations at XAN.

The accuracy of the aerosol pH predictions using ISORROPIA-lite was evaluated by comparing the observed with the predicted partitioning coefficient of  $\text{NH}_4^+$  ( $\epsilon(\text{NH}_4^+)$ ) and this comparison was possible only at PTR during winter when both  $\text{NH}_3$  and  $\text{NH}_4^+$  were measured. A useful way to assess the reliability and potential uncertainties of such models' predictions of aerosol pH is the comparison between measured and simulated gas-particle partitioning fractions of semivolatile species (Guo et al., 2016). Figure 4 shows the comparison of the observed and predicted  $\epsilon(\text{NH}_4^+)$  calculated for the case of PTR in winter. We focus on PTR since it was the only site where  $\text{NH}_3$  in-situ measurements were available making it a more suitable case for such comparison. The measurements and predictions of total ammonia are well correlated ( $R^2=0.78$ ) although the model underestimates by 30% the  $\epsilon(\text{NH}_4^+)$ . A sensitivity test and a re-evaluation of the model discussed in the supplementary section A3 (Fig S3) indicates that this small underestimation can be attributed to the uncertainty in the nitric acid levels. Sensitivity tests regarding the gas phase  $\text{NH}_3$  and  $\text{HNO}_3$  used to estimate aerosol pH are also provided (section 3.4). Overall,  $\text{PM}_{2.5}$  during winter varied acidic to moderately acidic with an average pH across all studied urban and urban background sites of  $3.57 \pm 0.44$ . The overall  $\text{PM}_{2.5}$  pH range across all 6 sites was from 1.72 to 5.14.

299

### 300 3.2.2 Summer

The seasonal variation of the acidity of  $\text{PM}_{2.5}$  was investigated at three of the sites, THI, FKL and IOA in which measurements were available for the summer 2019 PANACEA campaign. The mean  $\text{PM}_{2.5}$  composition is summarized in Table 1. During the whole period,  $\text{PM}_{2.5}$  at the three sites was acidic with a mean pH of  $1.35 \pm 0.18$  at THI,  $1.75 \pm 0.62$  at IOA and  $2.08 \pm 0.45$  pH at FKL (Figure 3c). At THI the  $\text{PM}_{2.5}$  pH was consistently low throughout the summer period with a minimum value of 1.13, and a maximum of 2. At IOA and FKL the  $\text{PM}_{2.5}$  pH was slightly higher than at THI. At FKL relative humidity levels increased the aerosol water content



and together with the relatively high  $K^+$  and  $Na^+$  levels led to higher aerosol pH. Higher  $Ca^{2+}$  and  $K^+$  levels at IOA and slightly higher sulfate levels at THI seemed to be the factors controlling the difference in the aerosol pH between these two sites. Overall, comparing the summertime aerosol pH levels at the three sites (Fig. 3c and S5), a uniformity can be observed with high aerosol acidity being the case on most of the days, dropping even below 0 at IOA as a result of increased temperature and sulfate levels and reduced aerosol water. FKL and IOA had similar aerosol pH levels since most of the major aerosol components had similar concentrations at the two sites. The higher  $Ca^{2+}$  at IOA was balanced by the higher  $Na^+$  in FKL.

### 3.2.3 Impact of organics

In order to investigate the potential effect of OA on the aerosol pH levels, ISORROPIA-lite was also run considering only the inorganic components of the aerosol (i.e. setting the OA concentration to zero). The mean difference between the aerosol pH calculated considering all aerosol components, including organics and the one accounting only for the inorganic content of  $PM_{2.5}$  is shown in Figs. 3b and d for winter and summer, respectively. The water associated with the OA should reduce the  $H^+$  concentration and therefore increase the aerosol pH (Kakavas et al., 2022). However, this expected increase in aerosol pH due to OA was not always found at all sites.

In winter at IOA, THI and PTR, the addition of aerosol water associated with the OA did not always increase the overall aerosol pH. In fact, a mean decrease of about 0.3 pH units was found at IOA, which had the highest OA concentrations among the 3 sites. Figure 5a depicts the aerosol water associated only with the inorganics along with the total one (i.e. including the OA water) and relative humidity and in Fig 5b the timeseries of the aerosol pH at IOA is shown in which again the one associated only with the inorganics and the one including the OA water (total aerosol pH) is depicted. The expected behavior of the aerosol pH as a result of the addition of the organics (an increase in aerosol pH is expected) is clear only at the end of January (from 26-01 to 29-01); the total aerosol pH was higher than the one when OA is absent (by 0.19 pH units on average). This was due to the high aerosol water content, which resulted from high relative humidity (above 80%). The addition of the OA increased aerosol water even more (Fig 5a). The decrease of aerosol pH when OA was present, was observed in all the other days in January where the addition of OA did not raise the aerosol water to levels that would result in increased pH. The concentration of  $H^+$  increased as a result of the addition of OA components, resulting in a more acidic aerosol (lower aerosol pH). The highest decrease in pH (mean decrease of 0.58 pH units) was observed in days where already relatively high aerosol pH occurred (inorganic aerosol pH above 4.5 units), while for the other cases the decrease was smaller (0.18 units mean decrease). Furthermore, the addition of OA affected the partitioning of the semivolatile species with a decrease in the gas phase (up to  $0.10 \mu g/m^3$  for  $NH_3$ , 0.18 for  $HNO_3$  and 0.12 for HCL), and a similar increase in the corresponding aerosol phase. At the other two sites the aerosol pH decreased by about 0.08 pH units at THI and 0.01 at PTR. At FKL, XAN and LAP a small increase in aerosol pH was found; 0.001, 0.05, 0.05 pH units increase respectively. In the summer, the pH increased at all sites when considering OA water, with the highest predicted increase of about 0.15 at IOA. At the other sites the aerosol pH increased by about 0.09 units at FKL and 0.11 at THI. Therefore, the effect of the organics on the pH at all sites was on average less than 0.3 units.

### 3.2.4 Main factors controlling seasonality of pH



A clear seasonal difference in acidity was observed at all sites. In summer  $PM_{2.5}$  at FKL was 1 pH unit more acidic than in winter. To determine the main drivers of aerosol pH seasonal variability, a series of sensitivity simulations were performed using the concentrations of aerosol components and meteorological conditions observed in winter and replacing each time one of them by its corresponding mean value in summer. Then, the difference in the estimated aerosol pH was calculated. The factors that were tested were chosen based on their difference between summer and winter and were: temperature, sulfates,  $TNH_3$  (sum of gas-phase  $NH_3$  and particulate  $NH_4^+$ ) and  $K^+$ . The results for FKL are shown in Fig. 6f and Table S4 as  $\Delta pH$ , that is the pH of the base case simulation minus that of the perturbation scenario. Sulfate was the main contributor to the change in aerosol acidity between summer and winter at FKL, where the  $2 \mu g m^{-3}$  concentration difference between the two seasons resulted in 1.66 units of pH difference. Total ammonia availability was the second most important factor with a mean  $\Delta pH$  of 0.39 followed by temperature (mean  $\Delta pH = 0.30$ ) and  $K^+$  (mean  $\Delta pH = 0.15$ ).

At IOA, aerosol average pH levels differed by 2.26 pH units between summer and winter with higher aerosol pH in winter (Fig. 6a). Simulations were performed using ISORROPIA-lite for nine factors: temperature, relative humidity,  $TNO_3$  (sum of gas-phase  $HNO_3$  and particulate  $NO_3^-$ ),  $TNH_3$ ,  $SO_4^{2-}$ ,  $Na^+$ ,  $K^+$ ,  $Ca^{2+}$  and OA. The results are shown in Fig. 6b and Table S5. Temperature ( $\Delta pH = 0.76$ ) and the availability of total nitric acid ( $\Delta pH = 0.98$ ) and ammonia ( $\Delta pH = 0.59$ ) had the greatest influence on the seasonal aerosol pH difference. The effect of  $K^+$  ( $\Delta pH = 0.53$ ), sulfates ( $\Delta pH = 0.45$ ) and  $Ca^{2+}$  ( $\Delta pH = 0.43$ ), followed by organics (0.22), RH (0.21) and  $Na^+$  (0.06) were also notable.

THI also exhibited a significant seasonal difference in the aerosol acidity with  $PM_{2.5}$  being approximately 2.6 times more acidic in summer than in winter (Fig. 6c). Eight sensitivity tests were conducted for the effect of: temperature, relative humidity,  $SO_4^{2-}$ ,  $K^+$ ,  $Ca^{2+}$ ,  $Na^+$ ,  $TNH_3$  and  $TNO_3$  on pH (Table S6, Fig. 6d). Sulfate was found to be the main contributor to the more acidic conditions in summer at THI with a mean absolute difference in pH (winter - summer),  $\Delta pH$ , of 2.8 units, followed by temperature and  $TNH_3$  with absolute  $\Delta pH$  of 0.42 and 0.48 units, respectively. The other factors contributed less to the seasonal difference in aerosol pH, with an absolute  $\Delta pH$  varying between 0.12 and 0.33 units.

371

### 372 3.3 Aerosol water

ISORROPIA-lite can also be used to calculate the contribution of each inorganic salt and organic fraction to the total aerosol water content. Fig. 7 depicts the average contributions of the various inorganic salts and of OA to the total aerosol water for all sites in winter (Fig. 7a) and summer (Fig. 7b).

In winter (Fig. 7a), OA contributed 60% to the total aerosol water at IOA and 55% at PTR. These were the two sites with the highest levels of OA mainly due to residential wood burning. At LAP and THI, OA was also the dominant aerosol component contributing to total aerosol water 37% and 33% respectively, while at XAN sulfate salts were associated with 42% and OA with 32% of the water. Focusing on the inorganic components alone, aerosol water was found to be controlled by nitrate and sulfate. Nitrate had the highest contributions to inorganic aerosol water at IOA (24%), THI (31%), LAP (30%) and PTR (21%).  $NH_4NO_3$  was the dominant salt at IOA, LAP and PTR; while at THI  $NaNO_3$  contributed 25% to the total water associated with inorganics along with  $NH_4NO_3$  (22%). The situation at FKL was different with chloride and sulfate being the major contributors to aerosol water (40% and 36% respectively), while OA had only a minor contribution (5%) due to its very low



385 concentration at this site. The dominant chloride salt at FKL was  $\text{NH}_4\text{Cl}$  contributing 31% to the total inorganic  
386 water while  $\text{Na}_2\text{SO}_4$  was the major sulfate salt, contributing 17%.

387 In summer in the three sites with available observations, sulfate dominated aerosol water (Fig. 7b) with  
388 contributions ranging from 70% at IOA to 80% at FKL and THI.  $(\text{NH}_4)_2\text{SO}_4$  was the dominant salt at all three  
389 sites, contributing more than half of the total water content at THI (58%) and 38% and 40% at IOA and FKL,  
390 respectively. The second most dominant aerosol component was OA with 19% contribution to the total aerosol  
391 water at THI, 27% at IOA and 14% at FKL.

392

### 393 3.4 Sensitivity of pH to $\text{NH}_3$ and $\text{HNO}_3$

394 Studies with ISORROPIA-II (Guo et al., 2015, Weber et al., 2016) have shown that neglecting gas-phase  $\text{NH}_3$  in  
395 the thermodynamic equilibrium calculation of pH results in an underestimation of at most one pH unit (Bougiatioti  
396 et al., 2016). Due to the lack of in situ measurements of the gas phase  $\text{NH}_3$  (except PTR) and  $\text{HNO}_3$  during the  
397 campaign periods, a sensitivity test was conducted varying the assumed concentrations of the gases that we used  
398 for the aerosol pH estimation. In detail, simulations with half and double the concentrations of  $\text{NH}_3$  and  $\text{HNO}_3$   
399 were conducted for all sites during both periods (winter and summer). The resulted difference in aerosol pH ( $\Delta\text{pH}$ )  
400 due to these altered gas phase concentrations are depicted in Fig. 8 and the mean values of  $\Delta\text{pH}$  for each simulation  
401 are summarized in Table S7 along with the concentrations of the gases for the base case scenarios (i.e. the  
402 concentrations used for the main simulations). For the case of  $\text{NH}_3$ , an average (across all sites and both periods)  
403 of 0.25 increase in aerosol pH was observed when double the amount of  $\text{NH}_3$  introduced to each system and the  
404 increase in pH ranged between 0.13 and 0.34 pH units. On the other hand, when half the amount of  $\text{NH}_3$  was used  
405 a smaller change was observed across the sites; the mean decrease in aerosol pH was -0.19 pH units while it  
406 ranged from -0.07 to -0.31 units. For the sensitivity simulations varying the amount of  $\text{HNO}_3$  the overall change  
407 in aerosol pH was much less distinct. The mean decrease in the pH of the aerosol was between 0.01 and 0.15 pH  
408 units when the concentration of  $\text{HNO}_3$  was doubled (the overall mean decrease was 0.06). Using half the  
409 concentration of  $\text{HNO}_3$  resulted in a mean increase ranging from 0.01 to 0.15 pH units.

410

### 411 3.5.1 Sensitivity of PM levels to ammonia and nitric acid availability

412 We used the framework developed by Nenes et al. (2020) that relates the levels of aerosol pH with the formation  
413 of aerosol nitrate (and ammonium), to investigate the sensitivity of the different aerosol systems studied here to  
414 the gas-phase concentrations of  $\text{NH}_3$  and  $\text{HNO}_3$ . The main parameters used in this framework that control the  
415 secondary inorganic particulate matter sensitivity are the aerosol pH, liquid water content and temperature. The  
416 conceptual idea is that there is a “sensitivity window” of pH levels in which the partitioning of nitrate shifts from  
417 nitrate being predominately gaseous to mostly in the aerosol phase. When acidity is below this pH sensitivity  
418 window, particulate nitrate is almost non-existent and consequently aerosol levels are insensitive to  $\text{HNO}_3$   
419 availability. In this case, aerosol reduction policies that only target nitric acid reduction cannot be effective (Nenes  
420 et al., 2020), as there is no nitrate in the aerosol phase. Based on these criteria, this framework defines  
421 characteristic levels of aerosol acidity at which the aerosol becomes insensitive to  $\text{NH}_3$  (or  $\text{HNO}_3$ ) levels and vice  
422 versa. Therefore, four possible regimes of PM sensitivity can be derived; i) neither  $\text{NH}_3$  nor  $\text{HNO}_3$  are important  
423 for PM formation, or PM formation is dominated by ii)  $\text{HNO}_3$ , iii) both  $\text{NH}_3$  and  $\text{HNO}_3$ , and iv)  $\text{NH}_3$  alone.



Figure 9 shows the  $PM_{2.5}$  sensitivity maps derived using this framework and the daily data at all stations in January 2020 (Fig. 9a) and at FKL, THI and IOA in summer (Fig. 9b) (34 days in total; in July and August 2019). Considering the average temperature across the 3 sites (Table S8) the pH sensitivity window for each of the two gases ( $NH_3$  and  $HNO_3$ ) was calculated as a function of aerosol water (LWC). The data that were used as well as the aerosol pH and water from the combination of the datasets from the 3 sites are given in Table S8.

During winter, an overall sensitivity of  $PM_{2.5}$  to  $HNO_3$  is found as most of the points of the sites reside above the blue line thus an increase in  $HNO_3$  concentration will lead to its partitioning to the aerosol phase as nitrate. On the other hand, most points are also above the red line indicating that  $PM_{2.5}$  is most insensitive to gas phase  $NH_3$ . Depending on the conditions and aerosol acidity levels, each site may have some days that deviate from the  $HNO_3$ -only sensitivity region. At FKL out of the 17 days where  $HNO_3$  sensitivity dominated, on 4 days  $PM_{2.5}$  was sensitive to both  $HNO_3$  and  $NH_3$  levels due to the slightly more acidic particles present. At THI  $PM_{2.5}$  was sensitive to  $HNO_3$  on all 27 days that were examined, except for two days in which  $NH_3$  sensitivity regime also occurred and characterized by lower aerosol pH values (2.05 and 2.13 pH units). At IOA as a consequence of the lower aerosol acidity,  $PM_{2.5}$  was (as expected) almost exclusively in the  $HNO_3$  sensitive regime where  $NH_3$  mass variations would not affect PM concentration. At IOA,  $NH_3$  availability was found to play a role in aerosol formation in two days when the aerosol water was very high in combination with the aerosol pH being slightly lower. Regions with more acidic particles i.e. XAN and LAP were also in some cases in the  $HNO_3$  and  $NH_3$  sensitive region.

During summer  $PM_{2.5}$  shifted out of the  $HNO_3$  only sensitive region at all three sites and  $NH_3$  started to play a more important role for the aerosol levels due to the more acidic conditions compared to winter. In many days at IOA and some at FKL the sensitivity to  $HNO_3$  and the insensitive regime also seemed to exist when extremely low aerosol water content was present. At THI  $PM_{2.5}$  sensitivity showed the least “dispersed” picture compared to the other sites, and  $PM_{2.5}$  was exclusively sensitive to  $NH_3$  availability due to the consistently high aerosol acidity conditions. Consequently, for the studied period the inorganic  $PM_{2.5}$  levels at THI would be reduced by controlling  $NO_x$  emissions in winter, and  $NH_3$  controls in summer. However, sulfate is the major inorganic  $PM_{2.5}$  component during the summer so the ammonia reductions would have a relatively small effect on the total fine PM.

451

### 3.5.2 Importance of semivolatiles for deposition

Aerosol acidity and water effects on the partitioning of  $HNO_3$  and  $NH_3$  are linked with the total deposition of these species, in both their gas and particulate forms. As  $HNO_3$  and  $NH_3$  are deposited about 10 times faster than their particulate forms ( $NO_3^-$ ,  $NH_4^+$ ), the partitioning between gas and particulate phase affects how fast  $HNO_3$ /  $NO_3^-$  or  $NH_3$ /  $NH_4^+$  are deposited (Nenes et al., 2021) and therefore the distance to which they are transported within the atmosphere before deposition (Baker et al., 2021). This gas-to-particle partitioning depends on the pH of the aerosol water and on the LWC of the aerosol (Guo et al., 2015). Therefore, “fast” and “slow” deposition regimes for  $HNO_3$  and  $NH_3$  can be defined as a function of aerosol pH and LWC. Figure 10 shows the reactive nitrogen (sum of  $TNO_3$  and  $TNH_3$ ) deposition regimes at the sites, where data were available both in winter (Fig. 10a) and summer (Fig. 10b), calculated using the average temperatures of the datasets for each season. Looking at the characterization of the deposition domains for all the studied sites during winter, a main difference can be observed



in terms of the nitrogen deposition velocity (Fig. 10a). At all sites,  $\text{NH}_3$  seems to always experience fast deposition. On the other hand, nitrate's deposition rate varies together with each ability for transport to other areas. IOA and PTR cases are almost exclusively in the  $\text{HNO}_3$  slow –  $\text{NH}_3$  fast regime due to the higher aerosol pH levels that enhance  $\text{HNO}_3$  partitioning to the particulate phase. The other sites are characterized by high deposition rates for both  $\text{NH}_3$  and  $\text{HNO}_3$ . In summer, the deposition is similarly characterized as fast for both  $\text{NH}_3$  and  $\text{HNO}_3$  at FKL, THI and IOA due to the higher acidity levels. The higher temperature in summer than in winter also favors the fast removal of both  $\text{HNO}_3$  and  $\text{NH}_3$ , with the exception of one day at IOA characterized by extremely low aerosol pH (below zero), where  $\text{NH}_3$  was present in the form of particulate  $\text{NH}_4^+$  and thus had a slow deposition velocity.

## Conclusions

This study was based on  $\text{PM}_{2.5}$  chemical composition observations in 6 regions of Greece (Finokalia, FKL; Thissio, THI; Patras, PTR; Ioannina, IOA; Xanthi, XAN; and Thessaloniki, LAP) during summer 2019 and winter 2019-2020 as part of the national research infrastructure PANACEA. The aerosol composition measurements together with the gas phase  $\text{NH}_3$ ,  $\text{HNO}_3$  data were used in the thermodynamic model ISORROPIA-lite to calculate the fine aerosol pH at all the sites and to determine its seasonal variation.

The pH levels of  $\text{PM}_{2.5}$  across Greece during winter ranged from 1.72 to 5.14. The highest pH values were estimated at IOA ( $4.08 \pm 0.42$ ) and PTR ( $3.70 \pm 0.45$ ) followed by THI ( $3.30 \pm 0.48$ ) and FKL ( $3.25 \pm 0.37$ ), while aerosols at XAN and LAP were the most acidic ( $2.81 \pm 0.53$  and  $3.01 \pm 0.31$ , respectively). The lowest acidity at IOA was associated with high  $\text{K}^+$  levels from biomass burning emissions in combination with high  $\text{Ca}^{2+}$  and  $\text{NH}_3$  and low temperatures. Similar factors ( $\text{NH}_3$  and cation levels) affected PTR aerosol pH. The aerosol acidity levels at the urban background site (THI) were similar to those at the coastal background site (FKL). High nonvolatile cation concentrations at FKL, together with elevated humidity levels resulted in a higher mean aerosol pH compared to the rural background site (XAN), which had slightly higher levels of sulfates than FKL.

In summer,  $\text{PM}_{2.5}$  was generally more acidic than in winter at the three sites studied (THI, IOA and FKL), with mean pH values of  $1.35 \pm 0.18$  (THI),  $1.75 \pm 0.62$  (IOA) and  $2.08 \pm 0.45$  units (FKL). pH in summer was lower than winter by 1 (FKL) to about 2 (THI and IOA) pH units. Sulfates drive the seasonal variation in aerosol pH at THI and FKL. At IOA, on the other hand, temperature together with  $\text{NH}_3$  and  $\text{HNO}_3$  availability were the main drivers of the seasonal difference in aerosol acidity, with  $\text{K}^+$ ,  $\text{Ca}^{2+}$ , and sulfates also contributing.

Organics contributed significantly to the total fine aerosol mass at all sites but FKL in winter. OA was found to be the main contributor to the total aerosol water at IOA and PTR (60% and 55% contribution, respectively) due to the OA levels in these sites, and the dominant contributor at THI and LAP (33% and 37% contribution respectively). During winter nitrate salts contributed more to the total aerosol water at IOA (24%), THI (31%), LAP (30%) and PTR (21%), with  $\text{NH}_4\text{NO}_3$  being the dominant salt present at IOA, LAP and PTR and  $\text{NaNO}_3$  at THI. The aerosol water content at XAN was dominated by sulfate (42%), with OA also contributing to the total aerosol water (32%). Chloride and sulfate contributed more to the aerosol water at FKL (40% and 36% respectively). During summer, sulfate salts contributed more to LWC at all sites (80% contribution at FKL and THI and 70% at IOA), with  $(\text{NH}_4)_2\text{SO}_4$  being the dominant species of the inorganic LWC at all three sites. At sites with higher aerosol pH (IOA, THI and PTR in winter), the water associated with the organics did not increase aerosol pH in most cases.



PM<sub>2.5</sub> mass was sensitive to the availability of total HNO<sub>3</sub> at all sites during winter. At LAP and XAN, PM mass was also found to be sensitive to NH<sub>3</sub>. In summer, PM at all three sites examined showed a strong sensitivity to NH<sub>3</sub> due to the low summertime aerosol pH. In some cases, the PM<sub>2.5</sub> concentrations at FKL and IOA appeared insensitive to both precursor species due to the low water content of the aerosols. PM sensitivity at THI in summer showed a clear dependence on NH<sub>3</sub>, reflecting the higher summertime aerosol acidity. Our results show that HNO<sub>3</sub> levels (could contribute to) regulate PM<sub>2.5</sub> mass concentration which however was mainly composed by OA and sulfate, hence policies targeted to reduce PM<sub>2.5</sub> levels in Greece would be more effective by reducing NO<sub>x</sub> emissions (i.e. transportation sector) in addition to OA and sulfate.

Finally, our analysis has shown that in Greece NH<sub>3</sub> deposition is fast, whereas deposition of HNO<sub>3</sub>/NO<sub>3</sub><sup>-</sup> may occur locally near the sources or remotely by long-range transport, depending on the environmental conditions. How future changes in the meteorological conditions and in air pollutant emissions will affect the aerosol pH and the factors controlling it, as well as atmospheric residence time and deposition of reactive nitrogen in the region, requires further investigation.

**Acknowledgements.** We acknowledge support of this work by the project “PANhellenic infrastructure for Atmospheric Composition and climate change” (MIS 5021516) which is implemented under the Action “Reinforcement of the Research and Innovation Infrastructure” ([http://www.antagonistikotita.gr/epanek\\_en/proskliseis.asp?id=28&cs=](http://www.antagonistikotita.gr/epanek_en/proskliseis.asp?id=28&cs=)), funded by the Operational Programme “Competitiveness, Entrepreneurship and Innovation” (NSRF 2014-2020) and co-financed by Greece and the European Union (European Regional Development Fund), by the European Research Council (ERC-2016-COG), Project Pyrogenic TRansformations Affecting Climate and Health (PyroTRACH-726165) by the Horizon-2020 Project FORCeS of the European Union under grant agreement No 821205 and by the Horizon-2020 project Research Infrastructures Services Reinforcing Air Quality Monitoring Capacities in European Urban & Industrial AreaS (RI-URBANS) grant agreement No. 101036245.

Colorblind friendly palettes were used to create the figures according to and described in (Crameri et al., 2020). More information about the abovementioned palettes can be found in <https://doi.org/10.5281/zenodo.8409685> (Crameri, 2018).

**Code availability.** ISORROPIA-lite is openly available at <https://www.epfl.ch/labs/lapi/models-and-software/isorropia/>

**Data availability.** Observational data are available upon request by the corresponding site principal investigator.

**Competing interests.** Some authors are members of the editorial board of journal Atmospheric Chemistry and Physics



539 Author contributions. AMN collected the data, performed the simulations and wrote the manuscript, MK  
540 conceived the study and supervised the work. MK and SP edited the manuscript, AN provided advice on the use  
541 of ISORROPIA model, and the frameworks by Nenes et al (2020 and 2021). MT, EL, KP, KT, IT, CK, FB, AK,  
542 KM, GK, NK, NH provided data; all authors provided comments on the manuscript.

543

## 544 References

545

546 Baker, A. R., Kanakidou, M., Nenes, A., Myriokefalitakis, S., Croot, P. L., Duce, R. A., Gao, Y., Guieu, C., Ito,  
547 A., Jickells, T. D., Mahowald, N. M., Middag, R., Perron, M. M. G., Sarin, M. M., Shelley, R., and Turner, D. R.:  
548 Changing atmospheric acidity as a modulator of nutrient deposition and ocean biogeochemistry, *Sci. Adv.*, 7,  
549 eabd8800, <https://doi.org/10.1126/sciadv.abd8800>, 2021.

550 Bougiatioti, A., Fountoukis, C., Kalivitis, N., Pandis, S. N., Nenes, A., and Mihalopoulos, N.: Cloud condensation  
551 nuclei measurements in the marine boundary layer of the Eastern Mediterranean: CCN closure and droplet growth  
552 kinetics, *Atmos. Chem. Phys.*, 9, 7053–7066, <https://doi.org/10.5194/acp-9-7053-2009>, 2009.

553 Bougiatioti, A., Nikolaou, P., Stavroulas, I., Kouvarakis, G., Weber, R., Nenes, A., Kanakidou, M., and  
554 Mihalopoulos, N.: Particle water and pH in the eastern Mediterranean: source variability and implications for  
555 nutrient availability, *Atmos. Chem. Phys.*, 16, 4579–4591, <https://doi.org/10.5194/acp-16-4579-2016>, 2016.

556 Clegg, S. L., Seinfeld, J. H., and Brimblecombe, P.: Thermodynamic modelling of aqueous aerosols containing  
557 electrolytes and dissolved organic compounds, *Journal of Aerosol Science*, 32, 713–738,  
558 [https://doi.org/10.1016/S0021-8502\(00\)00105-1](https://doi.org/10.1016/S0021-8502(00)00105-1), 2001.

559 Crameri, F.: Geodynamic diagnostics, scientific visualisation and StagLab 3.0, [https://doi.org/10.5194/gmd-2017-](https://doi.org/10.5194/gmd-2017-328)  
560 328, 20 February 2018.

561 Crameri, F., Shephard, G. E., and Heron, P. J.: The misuse of colour in science communication, *Nat Commun*,  
562 11, <https://doi.org/10.1038/s41467-020-19160-7>, 2020.

563 Ding, J., Zhao, P., Su, J., Dong, Q., Du, X., and Zhang, Y.: Aerosol pH and its driving factors in Beijing, *Atmos.*  
564 *Chem. Phys.*, 19, 7939–7954, <https://doi.org/10.5194/acp-19-7939-2019>, 2019.

565 Fang, T., Guo, H., Zeng, L., Verma, V., Nenes, A., and Weber, R. J.: Highly Acidic Ambient Particles, Soluble  
566 Metals, and Oxidative Potential: A Link between Sulfate and Aerosol Toxicity, *Environ. Sci. Technol.*, 51, 2611–  
567 2620, <https://doi.org/10.1021/acs.est.6b06151>, 2017.

568 Flocas, H., Kelessis, A., Helmis, C., Petrakakis, M., Zoumakis, M., and Pappas, K.: Synoptic and local scale  
569 atmospheric circulation associated with air pollution episodes in an urban Mediterranean area, *Theor Appl*  
570 *Climatol*, 95, 265–277, <https://doi.org/10.1007/s00704-008-0005-9>, 2009.

571 Florou, K., Papanastasiou, D. K., Pikridas, M., Kaltsonoudis, C., Louvaris, E., Gkatzelis, G. I., Patoulas, D.,  
572 Mihalopoulos, N., and Pandis, S. N.: The contribution of wood burning and other pollution sources to wintertime  
573 organic aerosol levels in two Greek cities, *Atmos. Chem. Phys.*, 17, 3145–3163, [https://doi.org/10.5194/acp-17-](https://doi.org/10.5194/acp-17-3145-2017)  
574 3145-2017, 2017.

575 Fountoukis, C. and Nenes, A.: ISORROPIA II: a computationally efficient thermodynamic equilibrium model for  
576  $K^+Ca^{2+}Mg^{2+}NH_4^+Na^+SO_4^{2-}NO_3^-Cl^-H_2O$  aerosols, *Atmos. Chem. Phys.*, 21, 2007.

577 Guo, H., Xu, L., Bougiatioti, A., Cerully, K. M., Capps, S. L., Hite, J. R., Carlton, A. G., Lee, S.-H., Bergin, M.  
578 H., Ng, N. L., Nenes, A., and Weber, R. J.: Fine-particle water and pH in the southeastern United States, *Atmos.*  
579 *Chem. Phys.*, 15, 5211–5228, <https://doi.org/10.5194/acp-15-5211-2015>, 2015.

580 Guo, H., Sullivan, A. P., Campuzano-Jost, P., Schroder, J. C., Lopez-Hilfiker, F. D., Dibb, J. E., Jimenez, J. L.,  
581 Thornton, J. A., Brown, S. S., Nenes, A., and Weber, R. J.: Fine particle pH and the partitioning of nitric acid



- 582 during winter in the northeastern United States, *J. Geophys. Res. Atmos.*, 121,  
583 <https://doi.org/10.1002/2016JD025311>, 2016.
- 584 Guo, H., Liu, J., Froyd, K. D., Roberts, J. M., Veres, P. R., Hayes, P. L., Jimenez, J. L., Nenes, A., and Weber, R.  
585 J.: Fine particle pH and gas–particle phase partitioning of inorganic species in Pasadena, California, during the  
586 2010 CalNex campaign, *Atmos. Chem. Phys.*, 17, 5703–5719, <https://doi.org/10.5194/acp-17-5703-2017>, 2017a.
- 587 Guo, H., Weber, R. J., and Nenes, A.: High levels of ammonia do not raise fine particle pH sufficiently to yield  
588 nitrogen oxide-dominated sulfate production, *Sci Rep*, 7, 12109, <https://doi.org/10.1038/s41598-017-11704-0>,  
589 2017b.
- 590 Guo, H., Otjes, R., Schlag, P., Kiendler-Scharr, A., Nenes, A., and Weber, R. J.: Effectiveness of ammonia  
591 reduction on control of fine particle nitrate, *Atmos. Chem. Phys.*, 18, 12241–12256, <https://doi.org/10.5194/acp-18-12241-2018>, 2018.
- 593 Hildebrandt, L., Kostenidou, E., Lanz, V. A., Prevot, A. S. H., Baltensperger, U., Mihalopoulos, N., Laaksonen,  
594 A., Donahue, N. M., and Pandis, S. N.: Sources and atmospheric processing of organic aerosol in the  
595 Mediterranean: insights from aerosol mass spectrometer factor analysis, *Atmos. Chem. Phys.*, 11, 12499–12515,  
596 <https://doi.org/10.5194/acp-11-12499-2011>, 2011.
- 597 Kakavas, S., Patoulias, D., Zakoura, M., Nenes, A., and Pandis, S. N.: Size-resolved aerosol pH over Europe  
598 during summer, *Atmos. Chem. Phys.*, 21, 799–811, <https://doi.org/10.5194/acp-21-799-2021>, 2021.
- 599 Kakavas, S., Pandis, S. N., and Nenes, A.: ISORROPIA-Lite: A Comprehensive Atmospheric Aerosol  
600 Thermodynamics Module for Earth System Models, *Tellus B: Chemical and Physical Meteorology*, 74, 1–23,  
601 <https://doi.org/10.16993/tellusb.33>, 2022.
- 602 Kalkavouras, P., Bougiatioti, A., Kalivitis, N., Stavroulas, I., Tombrou, M., Nenes, A., and Mihalopoulos, N.:  
603 Regional new particle formation as modulators of cloud condensation nuclei and cloud droplet number in the  
604 eastern Mediterranean, *Atmos. Chem. Phys.*, 19, 6185–6203, <https://doi.org/10.5194/acp-19-6185-2019>, 2019.
- 605 Kanakidou, M., Myriokefalitakis, S., and Tsigaridis, K.: Aerosols in atmospheric chemistry and biogeochemical  
606 cycles of nutrients, *Environ. Res. Lett.*, 13, 063004, <https://doi.org/10.1088/1748-9326/aabcbd>, 2018.
- 607 Kaskaoutis, D. G., Grivas, G., Theodosi, C., Tsagkaraki, M., Paraskevopoulou, D., Stavroulas, I., Liakakou, E.,  
608 Gkikas, A., Hatzianastassiou, N., Wu, C., Gerasopoulos, E., and Mihalopoulos, N.: Carbonaceous Aerosols in  
609 Contrasting Atmospheric Environments in Greek Cities: Evaluation of the EC-tracer Methods for Secondary  
610 Organic Carbon Estimation, *Atmosphere*, 11, 161, <https://doi.org/10.3390/atmos11020161>, 2020.
- 611 Kaskaoutis, D. G., Grivas, G., Oikonomou, K., Tavernarakis, P., Papoutsidaki, K., Tsagkaraki, M., Stavroulas, I.,  
612 Zampas, P., Paraskevopoulou, D., Bougiatioti, A., Liakakou, E., Gavrouzou, M., Dumka, U. C., Hatzianastassiou,  
613 N., Sciare, J., Gerasopoulos, E., and Mihalopoulos, N.: Impacts of severe residential wood burning on atmospheric  
614 processing, water-soluble organic aerosol and light absorption, in an inland city of Southeastern Europe,  
615 *Atmospheric Environment*, 280, 119139, <https://doi.org/10.1016/j.atmosenv.2022.119139>, 2022.
- 616 Kastelis, N. and Kourtidis, K.: Characteristics of the atmospheric electric field and correlation with CO<sub>2</sub> at a rural  
617 site in southern Balkans, *Earth Planet Sp.*, 68, 3, <https://doi.org/10.1186/s40623-016-0379-3>, 2016.
- 618 Kostenidou, E., Florou, K., Kaltsonoudis, C., Tsiplikiotou, M., Vratolis, S., Eleftheriadis, K., and Pandis, S. N.:  
619 Sources and chemical characterization of organic aerosol during the summer in the eastern Mediterranean, *Atmos.*  
620 *Chem. Phys.*, 15, 11355–11371, <https://doi.org/10.5194/acp-15-11355-2015>, 2015.
- 621 Lemou, A., Rabhi, L., Merabet, H., Ladji, R., Nicolas, J. B., Bonnaire, N., Mustapha, M. A., Dilmi, R., Sciare, J.,  
622 Mihalopoulos, N., and Yassaa, N.: Chemical characterization of fine particles (PM<sub>2.5</sub>) at a coastal site in the  
623 South Western Mediterranean during the ChArMex experiment, *Environ Sci Pollut Res*, 27, 20427–20445,  
624 <https://doi.org/10.1007/s11356-020-08168-7>, 2020.
- 625 Liakakou, E., Fournziou, L., Paraskevopoulou, D., Speyer, O., Lianou, M., Grivas, G., Myriokefalitakis, S., and  
626 Mihalopoulos, N.: High-Resolution Measurements of SO<sub>2</sub>, HNO<sub>3</sub> and HCl at the Urban Environment of Athens,



- 627 Greece: Levels, Variability and Gas to Particle Partitioning, *Atmosphere*, 13, 218,  
628 <https://doi.org/10.3390/atmos13020218>, 2022.
- 629 Liu, M., Song, Y., Zhou, T., Xu, Z., Yan, C., Zheng, M., Wu, Z., Hu, M., Wu, Y., and Zhu, T.: Fine particle pH  
630 during severe haze episodes in northern China: Fine Particle pH During Haze Episodes, *Geophys. Res. Lett.*, 44,  
631 5213–5221, <https://doi.org/10.1002/2017GL073210>, 2017.
- 632 Masiol, M., Squizzato, S., Formenton, G., Khan, M. B., Hopke, P. K., Nenes, A., Pandis, S. N., Tositti, L.,  
633 Benetello, F., Visin, F., and Pavoni, B.: Hybrid multiple-site mass closure and source apportionment of PM<sub>2.5</sub>  
634 and aerosol acidity at major cities in the Po Valley, *Science of The Total Environment*, 704, 135287,  
635 <https://doi.org/10.1016/j.scitotenv.2019.135287>, 2020.
- 636 Mihalopoulos, N., Stephanou, E., Kanakidou, M., Pilitsidis, S., and Bousquet, P.: Tropospheric aerosol ionic  
637 composition in the Eastern Mediterranean region, *Tellus B*, 49, 314–326, <https://doi.org/10.1034/j.1600-0889.49.issue3.7.x>, 1997.
- 639 Nenes, A., Pandis, S. N., Weber, R. J., and Russell, A.: Aerosol pH and liquid water content determine when  
640 particulate matter is sensitive to ammonia and nitrate availability, *Atmos. Chem. Phys.*, 20, 3249–3258,  
641 <https://doi.org/10.5194/acp-20-3249-2020>, 2020.
- 642 Nenes, A., Pandis, S. N., Kanakidou, M., Russell, A. G., Song, S., Vasilakos, P., and Weber, R. J.: Aerosol acidity  
643 and liquid water content regulate the dry deposition of inorganic reactive nitrogen, *Atmos. Chem. Phys.*, 21, 6023–  
644 6033, <https://doi.org/10.5194/acp-21-6023-2021>, 2021.
- 645 Paglione, M., Decesari, S., Rinaldi, M., Tarozzi, L., Manarini, F., Gilardoni, S., Facchini, M. C., Fuzzi, S., Bacco,  
646 D., Trentini, A., Pandis, S. N., and Nenes, A.: Historical Changes in Seasonal Aerosol Acidity in the Po Valley  
647 (Italy) as Inferred from Fog Water and Aerosol Measurements, *Environ. Sci. Technol.*, 55, 7307–7315,  
648 <https://doi.org/10.1021/acs.est.1c00651>, 2021.
- 649 Pikridas, M., Bougiatioti, A., Hildebrandt, L., Engelhart, G. J., Kostenidou, E., Mohr, C., Prévôt, A. S. H.,  
650 Kouvarakis, G., Zampas, P., Burkhardt, J. F., Lee, B.-H., Psichoudaki, M., Mihalopoulos, N., Pilinis, C., Stohl,  
651 A., Baltensperger, U., Kulmala, M., and Pandis, S. N.: The Finokalia Aerosol Measurement Experiment – 2008  
652 (FAME-08): an overview, *Atmos. Chem. Phys.*, 10, 6793–6806, <https://doi.org/10.5194/acp-10-6793-2010>, 2010.
- 653 Pikridas, M., Tasoglou, A., Florou, K., and Pandis, S. N.: Characterization of the origin of fine particulate matter  
654 in a medium size urban area in the Mediterranean, *Atmospheric Environment*, 80, 264–274,  
655 <https://doi.org/10.1016/j.atmosenv.2013.07.070>, 2013.
- 656 Powley, H. R., Cappellen, P. V., and Krom, M. D.: Nutrient Cycling in the Mediterranean Sea: The Key to  
657 Understanding How the Unique Marine Ecosystem Functions and Responds to Anthropogenic Pressures, in:  
658 *Mediterranean Identities - Environment, Society, Culture*, edited by: Fuerst-Bjelis, B., InTech,  
659 <https://doi.org/10.5772/intechopen.70878>, 2017.
- 660 Psichoudaki, M., Nenes, A., Florou, K., Kaltsonoudis, C., and Pandis, S. N.: Hygroscopic properties of  
661 atmospheric particles emitted during wintertime biomass burning episodes in Athens, *Atmospheric Environment*,  
662 178, 66–72, <https://doi.org/10.1016/j.atmosenv.2018.01.004>, 2018.
- 663 Putaud, J.-P., Raes, F., Van Dingenen, R., Brüggemann, E., Facchini, M.-C., Decesari, S., Fuzzi, S., Gehrig, R.,  
664 Hüglin, C., Laj, P., Lorbeer, G., Maenhaut, W., Mihalopoulos, N., Müller, K., Querol, X., Rodriguez, S.,  
665 Schneider, J., Spindler, G., Brink, H. T., Tørseth, K., and Wiedensohler, A.: A European aerosol  
666 phenomenology—2: chemical characteristics of particulate matter at kerbside, urban, rural and background sites  
667 in Europe, *Atmospheric Environment*, 38, 2579–2595, <https://doi.org/10.1016/j.atmosenv.2004.01.041>, 2004.
- 668 Pye, H. O. T., Nenes, A., Alexander, B., Ault, A. P., Barth, M. C., Clegg, S. L., Collett, J. L., Fahey, K. M.,  
669 Hennigan, C. J., Herrmann, H., Kanakidou, M., Kelly, J. T., Ku, I. T., Faye McNeill, V., Riemer, N., Schaefer,  
670 T., Shi, G., Tilgner, A., Walker, J. T., Wang, T., Weber, R., Xing, J., Zaveri, R. A., and Zuend, A.: The acidity of  
671 atmospheric particles and clouds, *Atmospheric Chemistry and Physics*, 20, 4809–4888,  
672 <https://doi.org/10.5194/acp-20-4809-2020>, 2020a.



- 673 Pye, H. O. T., Nenes, A., Alexander, B., Ault, A. P., Barth, M. C., Clegg, S. L., Collett Jr., J. L., Fahey, K. M.,  
674 Hennigan, C. J., Herrmann, H., Kanakidou, M., Kelly, J. T., Ku, I.-T., McNeill, V. F., Riener, N., Schaefer, T.,  
675 Shi, G., Tilgner, A., Walker, J. T., Wang, T., Weber, R., Xing, J., Zaveri, R. A., and Zuend, A.: The acidity of  
676 atmospheric particles and clouds, *Atmos. Chem. Phys.*, 20, 4809–4888, [https://doi.org/10.5194/acp-20-4809-](https://doi.org/10.5194/acp-20-4809-2020)  
677 2020, 2020b.
- 678 Sciare, J., Oikonomou, K., Favez, O., Liakakou, E., Markaki, Z., Cachier, H., and Mihalopoulos, N.: Long-term  
679 measurements of carbonaceous aerosols in the Eastern Mediterranean: evidence of long-range transport of  
680 biomass burning, *Atmos. Chem. Phys.*, 2008.
- 681 Seinfeld, J. H. and Pandis, S. N.: *Atmospheric chemistry and physics: from air pollution to climate change*, 2nd  
682 ed., J. Wiley, Hoboken, N.J, 1203 pp., 2006.
- 683 Shephard, M. W. and Cady-Pereira, K. E.: Cross-track Infrared Sounder (CrIS) satellite observations of  
684 tropospheric ammonia, *Atmos. Meas. Tech.*, 8, 1323–1336, <https://doi.org/10.5194/amt-8-1323-2015>, 2015.
- 685 Shephard, M. W., Dammers, E., Cady-Pereira, K. E., Kharol, S. K., Thompson, J., Gainariu-Matz, Y., Zhang, J.,  
686 McLinden, C. A., Kovachik, A., Moran, M., Bittman, S., Sioris, C. E., Griffin, D., Alvarado, M. J., Lonsdale, C.,  
687 Savic-Jovicic, V., and Zheng, Q.: Ammonia measurements from space with the Cross-track Infrared Sounder:  
688 characteristics and applications, *Atmos. Chem. Phys.*, 20, 2277–2302, <https://doi.org/10.5194/acp-20-2277-2020>,  
689 2020.
- 690 Shi, G., Xu, J., Peng, X., Xiao, Z., Chen, K., Tian, Y., Guan, X., Feng, Y., Yu, H., Nenes, A., and Russell, A. G.:  
691 pH of Aerosols in a Polluted Atmosphere: Source Contributions to Highly Acidic Aerosol, *Environ. Sci. Technol.*,  
692 51, 4289–4296, <https://doi.org/10.1021/acs.est.6b05736>, 2017.
- 693 Squizzato, S., Masiol, M., Brunelli, A., Pistollato, S., Tarabotti, E., Rampazzo, G., and Pavoni, B.: Factors  
694 determining the formation of secondary inorganic aerosol: a case study in the Po Valley (Italy), *Atmos. Chem.*  
695 *Phys.*, 13, 1927–1939, <https://doi.org/10.5194/acp-13-1927-2013>, 2013.
- 696 Stavroulas, I., Bougiatioti, A., Grivas, G., Paraskevopoulou, D., Tsagkaraki, M., Zarnpas, P., Liakakou, E.,  
697 Gerasopoulos, E., and Mihalopoulos, N.: Sources and processes that control the submicron organic aerosol  
698 composition in an urban Mediterranean environment (Athens): a high temporal-resolution chemical composition  
699 measurement study, *Atmos. Chem. Phys.*, 19, 901–919, <https://doi.org/10.5194/acp-19-901-2019>, 2019.
- 700 Tao, Y. and Murphy, J. G.: The sensitivity of PM<sub>2.5</sub> acidity to meteorological parameters  
701 and chemical composition changes: 10-year records from six Canadian monitoring sites, *Atmos. Chem. Phys.*, 19,  
702 9309–9320, <https://doi.org/10.5194/acp-19-9309-2019>, 2019.
- 703 Theodosi, C., Markaki, Z., and Mihalopoulos, N.: Iron speciation, solubility and temporal variability in wet and  
704 dry deposition in the Eastern Mediterranean, *Marine Chemistry*, 120, 100–107,  
705 <https://doi.org/10.1016/j.marchem.2008.05.004>, 2008.
- 706 Tsiflikiotou, M. A., Kostenidou, E., Papanastasiou, D. K., Patoulas, D., Zarnpas, P., Paraskevopoulou, D.,  
707 Diapouli, E., Kaltsonoudis, C., Florou, K., Bougiatioti, A., Stavroulas, I., Theodosi, C., Kouvarakis, G., Vasilatou,  
708 V., Siakavaras, D., Biskos, G., Pilinis, C., Eleftheriadis, K., Gerasopoulos, E., Mihalopoulos, N., and Pandis, S.  
709 N.: Summertime particulate matter and its composition in Greece, *Atmospheric Environment*, 213, 597–607,  
710 <https://doi.org/10.1016/j.atmosenv.2019.06.013>, 2019.
- 711 Vierke, L., Ahrens, L., Shoeib, M., Palm, W.-U., Webster, E. M., Ellis, D. A., Ebinghaus, R., and Harner, T.: In  
712 situ air–water and particle–water partitioning of perfluorocarboxylic acids, perfluorosulfonic acids and  
713 perfluorooctyl sulfonamide at a wastewater treatment plant, *Chemosphere*, 92, 941–948,  
714 <https://doi.org/10.1016/j.chemosphere.2013.02.067>, 2013.
- 715 Warner, J. X., Wei, Z., Strow, L. L., Dickerson, R. R., and Nowak, J. B.: The global tropospheric ammonia  
716 distribution as seen in the 13-year AIRS measurement record, *Atmos. Chem. Phys.*, 16, 5467–5479,  
717 <https://doi.org/10.5194/acp-16-5467-2016>, 2016.
- 718 Weber, R. J., Guo, H., Russell, A. G., and Nenes, A.: High aerosol acidity despite declining atmospheric sulfate  
719 concentrations over the past 15 years, *Nature Geosci.*, 9, 282–285, <https://doi.org/10.1038/ngeo2665>, 2016.



- 720 Wexler, A. S.: Atmospheric aerosol models for systems including the ions  $\text{H}^+$ ,  $\text{NH}_4^+$ ,  $\text{Na}^+$ ,  $\text{SO}_4^{2-}$ ,  $\text{NO}_3^-$ ,  
721  $\text{Cl}^-$ ,  $\text{Br}^-$ , and  $\text{H}_2\text{O}$ , *J. Geophys. Res.*, 107, 4207, <https://doi.org/10.1029/2001JD000451>, 2002.
- 722 Zaveri, R. A., Easter, R. C., Fast, J. D., and Peters, L. K.: Model for Simulating Aerosol Interactions and Chemistry  
723 (MOSAIC), *J. Geophys. Res.*, 113, D13204, <https://doi.org/10.1029/2007JD008782>, 2008.
- 724 Zhang, A., Wang, Y., Zhang, Y., Weber, R. J., Song, Y., Ke, Z., and Zou, Y.: Modeling the global radiative effect  
725 of brown carbon: a potentially larger heating source in the tropical free troposphere than black carbon, *Atmos.*  
726 *Chem. Phys.*, 20, 1901–1920, <https://doi.org/10.5194/acp-20-1901-2020>, 2020.

727



## FIGURES AND TABLES

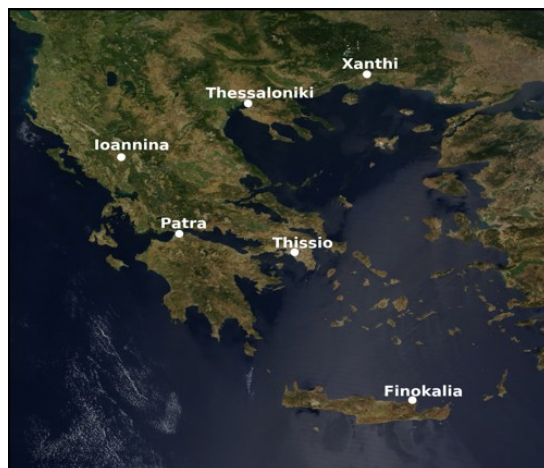


Figure 1: Map of the region of Greece and the sampling sites. From south to north, Finokalia (FKL), Thissio (THI), Patras (PTR), Ioannina (IOA), Thessaloniki (LAP) and Xanthi (XAN). Original satellite image of Greece obtained from ([https://upload.wikimedia.org/wikipedia/commons/9/92/Satellite\\_image\\_of\\_Greece.jpg](https://upload.wikimedia.org/wikipedia/commons/9/92/Satellite_image_of_Greece.jpg))

Table 1: Descriptive statistics (mean  $\pm$  stdev) for the chemical composition of PM<sub>2.5</sub> during the winter and summer PANACEA campaigns. *OA* is the *organic aerosol* derived from OC measurements and a ratio of *OA/OC* of 1.8. Meteorological conditions are also provided. (\*) The aerosol pH and LWC calculated with ISORROPIA-lite are also provided (n= number of days).

Observations	FKL		THI		PTR		IOA		LAP	XAN
$\mu\text{g}/\text{m}^3$	winter	summer	winter	summer	winter	winter	summer	summer	winter	winter
OA	0.69 $\pm$ 0.49	2.91 $\pm$ 1.10	4.77 $\pm$ 4.53	7.51 $\pm$ 5.27	17.35 $\pm$ 7.61	50.36 $\pm$ 34.46	5.06 $\pm$ 1.77	12.45 $\pm$ 7.97	6.78 $\pm$ 3.33	
Na <sup>+</sup>	0.39 $\pm$ 0.25	0.46 $\pm$ 0.33	0.24 $\pm$ 0.11	0.17 $\pm$ 0.13	0.32 $\pm$ 0.30	0.19 $\pm$ 0.11	0.12 $\pm$ 0.06	0.46 $\pm$ 0.49	0.14 $\pm$ 0.38	
NH <sub>4</sub> <sup>+</sup>	0.20 $\pm$ 0.25	0.99 $\pm$ 0.37	0.40 $\pm$ 0.25	1.46 $\pm$ 0.50	0.67 $\pm$ 0.43	1.12 $\pm$ 0.81	0.79 $\pm$ 0.33	1.04 $\pm$ 0.76	0.75 $\pm$ 0.58	
K <sup>+</sup>	0.18 $\pm$ 0.24	0.25 $\pm$ 0.13	0.29 $\pm$ 0.24	0.12 $\pm$ 0.05	0.75 $\pm$ 0.43	1.45 $\pm$ 1.00	0.27 $\pm$ 0.18	0.37 $\pm$ 0.17	0.30 $\pm$ 0.16	
Ca <sup>2+</sup>	0.27 $\pm$ 0.40	0.18 $\pm$ 0.14	0.23 $\pm$ 0.24	0.23 $\pm$ 0.20	0.34 $\pm$ 0.44	0.96 $\pm$ 0.78	0.55 $\pm$ 0.25	0.33 $\pm$ 0.11	0.17 $\pm$ 0.06	
Mg <sup>2+</sup>	0.10 $\pm$ 0.12	0.06 $\pm$ 0.03	0.02 $\pm$ 0.02	0.06 $\pm$ 0.01	0.03 $\pm$ 0.04	0.03 $\pm$ 0.02	0.04 $\pm$ 0.01	0.04 $\pm$ 0.01	0.04 $\pm$ 0.02	
SO <sub>4</sub> <sup>2-</sup>	1.30 $\pm$ 0.59	3.71 $\pm$ 1.18	0.77 $\pm$ 0.43	4.42 $\pm$ 1.59	1.78 $\pm$ 0.90	2.77 $\pm$ 1.42	3.27 $\pm$ 1.02	2.05 $\pm$ 1.00	1.90 $\pm$ 1.36	
NO <sub>3</sub> <sup>-</sup>	0.30 $\pm$ 0.30	0.14 $\pm$ 0.11	0.66 $\pm$ 0.50	0.16 $\pm$ 0.09	1.39 $\pm$ 0.78	3.66 $\pm$ 2.73	0.17 $\pm$ 0.07	2.01 $\pm$ 1.71	0.70 $\pm$ 0.58	
Cl <sup>-</sup>	0.37 $\pm$ 0.47	0.31 $\pm$ 0.30	0.40 $\pm$ 0.19	0.40 $\pm$ 0.12	0.25 $\pm$ 0.27	0.61 $\pm$ 0.38	0.26 $\pm$ 0.07	0.33 $\pm$ 0.14	0.40 $\pm$ 0.18	
T (°C)	11.83 $\pm$ 2.74	24.84 $\pm$ 1.66	10.64 $\pm$ 3.22	28.97 $\pm$ 1.90	11.14 $\pm$ 2.36	7.43 $\pm$ 2.52	26.86 $\pm$ 2.60	9.94 $\pm$ 2.65	8.62 $\pm$ 2.90	
RH (%)	72.03 $\pm$ 9.68	65.82 $\pm$ 9.66	65.85 $\pm$ 11.65	46.04 $\pm$ 6.69	64.66 $\pm$ 11.97	68.06 $\pm$ 20.25	51.59 $\pm$ 9.73	57.62 $\pm$ 13.17	62.43 $\pm$ 16.88	
Month (number of samples)	January (n=16)	July & August (n=34)	January (n=27)	July & August (n=34)	January (n=16)	January (n=27)	July & August (n=34)	January (n=4)	January (n=26)	
pH*	3.25 $\pm$ 0.37	2.08 $\pm$ 0.37	3.30 $\pm$ 0.48	1.38 $\pm$ 0.18	3.70 $\pm$ 0.45	4.08 $\pm$ 0.42	1.82 $\pm$ 0.65	3.01 $\pm$ 0.31	2.81 $\pm$ 0.53	
LWC ( $\mu\text{g}/\text{m}^3$ )*	6.85 $\pm$ 3.65	5.85 $\pm$ 3.05	3.06 $\pm$ 2.96	3.34 $\pm$ 1.62	7.00 $\pm$ 5.36	56.61 $\pm$ 127.59	1.97 $\pm$ 0.79	29.68 $\pm$ 32.67	4.57 $\pm$ 4.29	

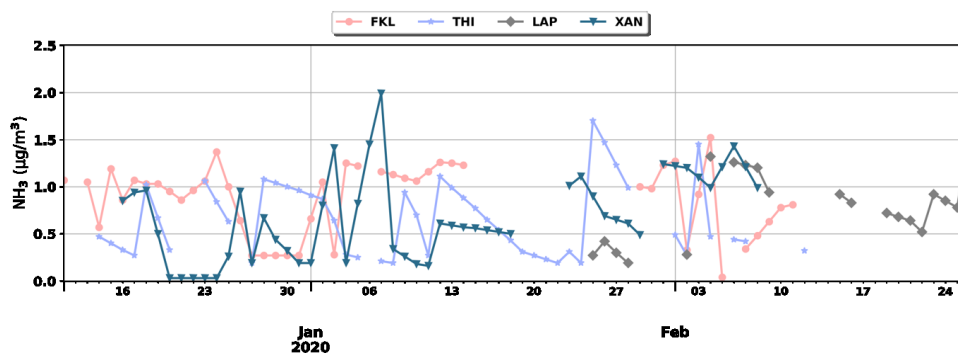


Figure 2: Daily surface  $\text{NH}_3$  concentrations during the winter of 2019-2020 as derived from the Cross-track Infrared Sounder (CrIS) instrument for FKL, THI, LAP and XAN.

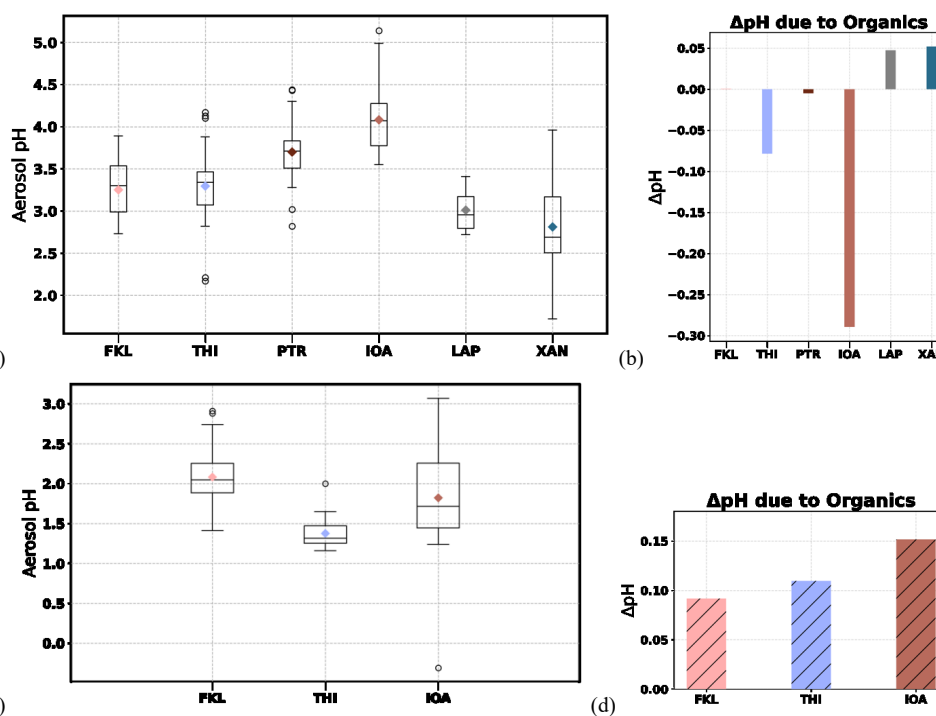


Figure 3: a) and c) total aerosol pH (meaning the aerosol pH associated with inorganics and organics) derived using ISORROPIA-lite in January 2020 and summer 2019 respectively, b) and d)  $\Delta\text{pH}$  = total aerosol pH – inorganic aerosol pH both derived from ISORROPIA-lite in January 2020 and summer 2019 respectively. The inorganic aerosol pH was derived by setting the organic concentration and hygroscopicity as zero.

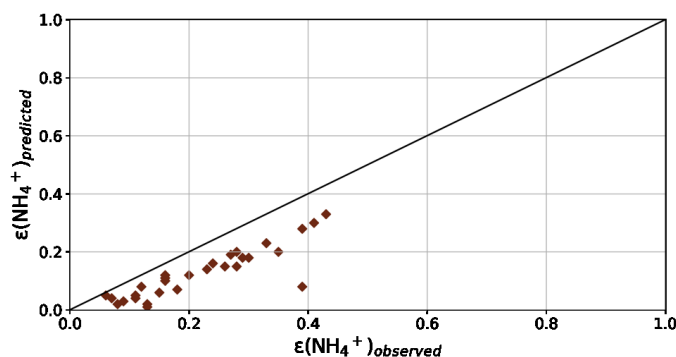


Figure 4: Evaluation of the ISORROPIA-lite results for the case of PTR in winter. Comparison of the partitioning coefficient of  $\text{NH}_4^+$  calculated from measurements with that from the predicted concentrations derived from the model ( $R^2 = 0.78$  and  $y = 0.70x - 0.03$ ). The partitioning coefficient is defined as  $\varepsilon(\text{NH}_4^+) = \text{NH}_4^+ / (\text{NH}_4^+ + \text{NH}_3)$ . The black line shows the 1:1 ratio.

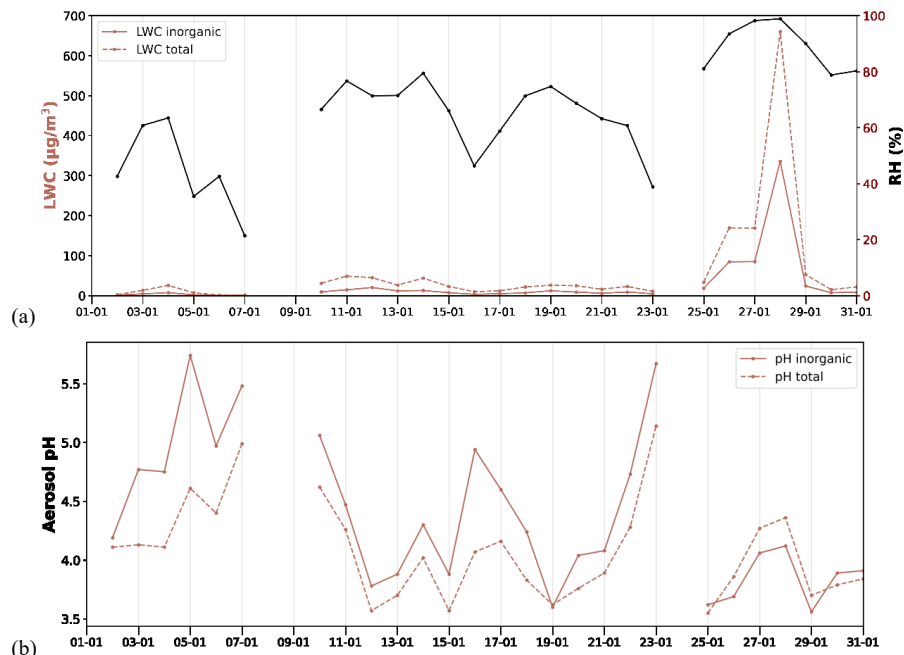


Figure 5: (a) Aerosol liquid water content at IOA in January 2020 as derived from ISORROPIA-lite associated with inorganics (inorganic, red line), associated with both inorganics and organics (total, red-dashed line) and relative humidity levels (secondary y axis, black line). (b) Inorganic (red line) and total (red dashed line, associated with inorganics and organics) aerosol pH at IOA in January 2020.

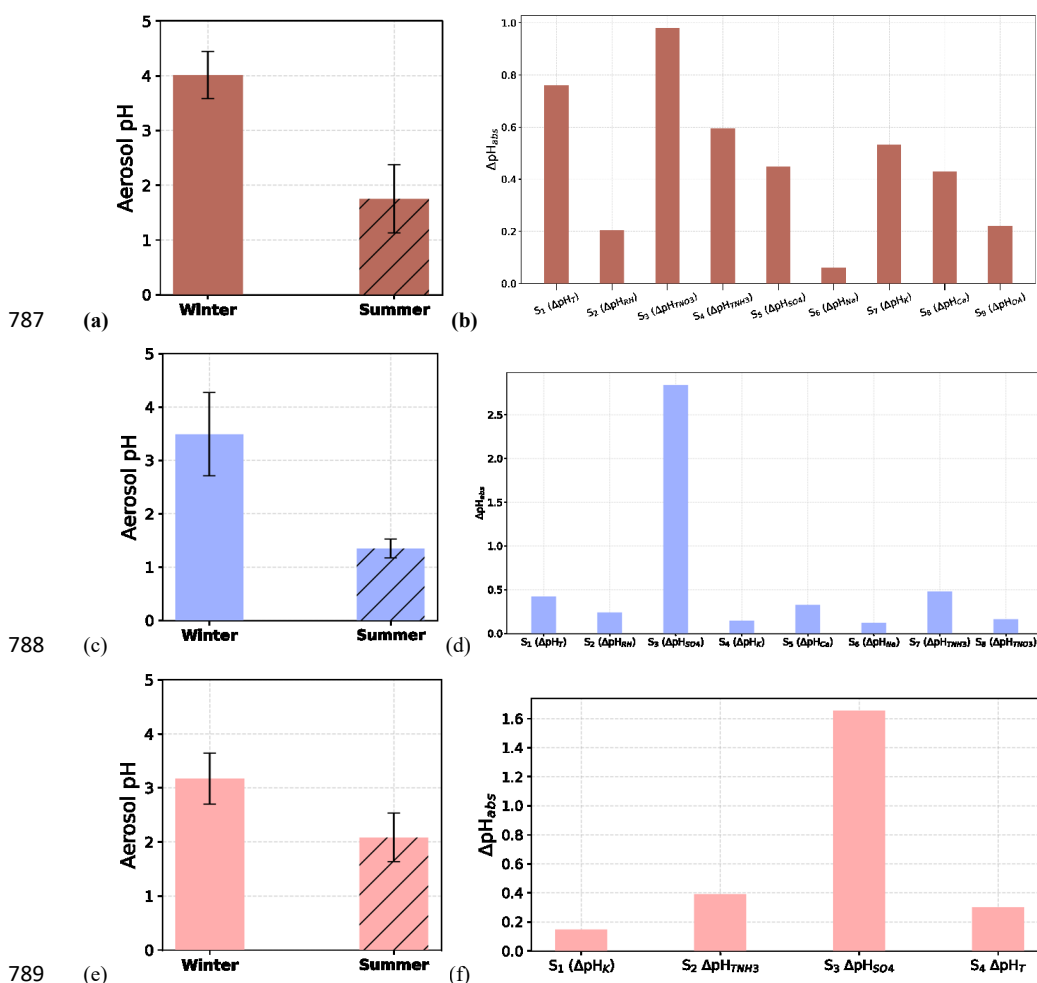


783

784

785

786



789

Figure 6: Mean fine aerosol pH in winter and in summer at (a) IOA (c) THI, (e) FKL and the respective sensitivity results for winter conducted for each site (Tables S4-S6).  $\Delta pH_{abs} = |pH_{winter} - pH_{winter(summerX)}|$ , where summerX is (b) for IOA: the mean summer temperature (first simulation,  $S_1$ ), relative humidity ( $S_2$ ),  $TNO_3$  ( $S_3$ ),  $TNH_3$  ( $S_4$ ),  $SO_4^{2-}$  ( $S_5$ ),  $Na^+$  ( $S_6$ ),  $K^+$  ( $S_7$ ),  $Ca^{2+}$  ( $S_8$ ) and  $OA$  concentration ( $S_9$ ) (d) for THI: the mean summer temperature ( $S_1$ ), relative humidity ( $S_2$ ),  $SO_4^{2-}$  ( $S_3$ ),  $K^+$  ( $S_4$ ),  $Ca^{2+}$  ( $S_5$ ),  $Na^+$  ( $S_6$ ),  $TNH_3$  ( $S_7$ ) and  $TNO_3$  ( $S_8$ ) concentration and (e) for FKL: the mean summer  $K^+$  ( $S_1$ ),  $TNH_3$  concentration ( $S_2$ ),  $SO_4^{2-}$  concentration ( $S_3$ ) and temperature ( $S_4$ ).

790

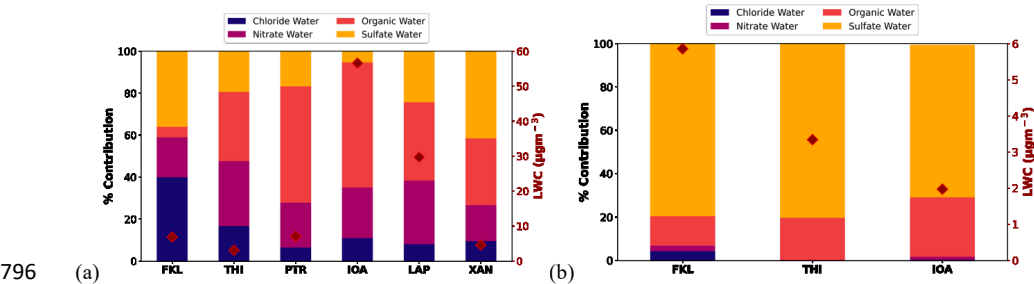
791

792

793

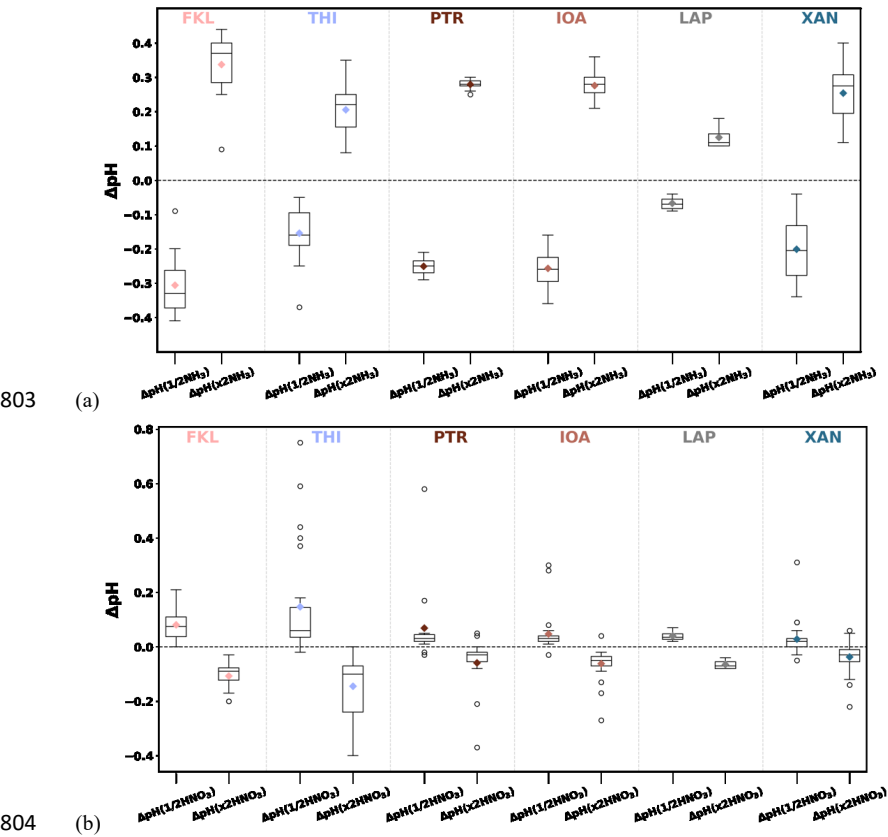
794

795



797 Figure 7: Averaged aerosol liquid water content (LWC) for all sites in winter, January 2020 (a) and summer, July and  
798 August 2019 (b) expressed as the contribution of each chemical aerosol salt group considering both the inorganics and  
799 organics at the observational sites shown in Fig. 1 (left axis). Aerosol water mean concentrations are shown with  
800 rhombus in each plot (right axis).

801  
802



804

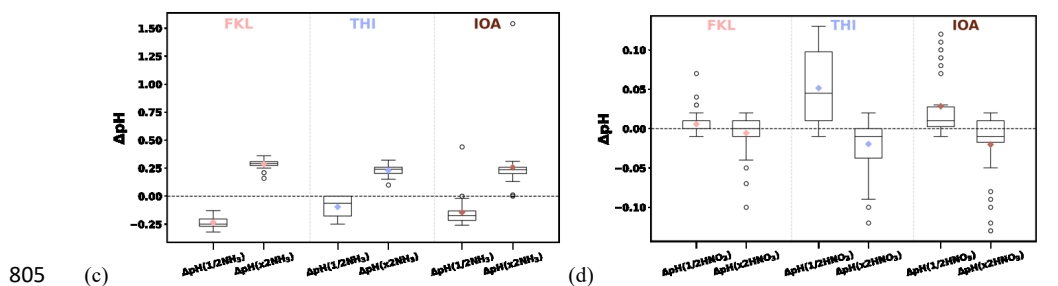


Figure 8: Sensitivity of pH estimation to gas phase  $NH_3$  and  $HNO_3$  concentrations. (a) and (b) are the wintertime (January) simulations for  $NH_3$  and  $HNO_3$  tests respectively and (c) and (d) for the summertime ones. Each graph shows the difference in pH when using half or double the concentration of the respective gas compared to the original pH at each site. ( $\Delta pH = pH_{1/2gas} - pH_{original}$  and  $\Delta pH = pH_{2gas} - pH_{original}$  respectively).

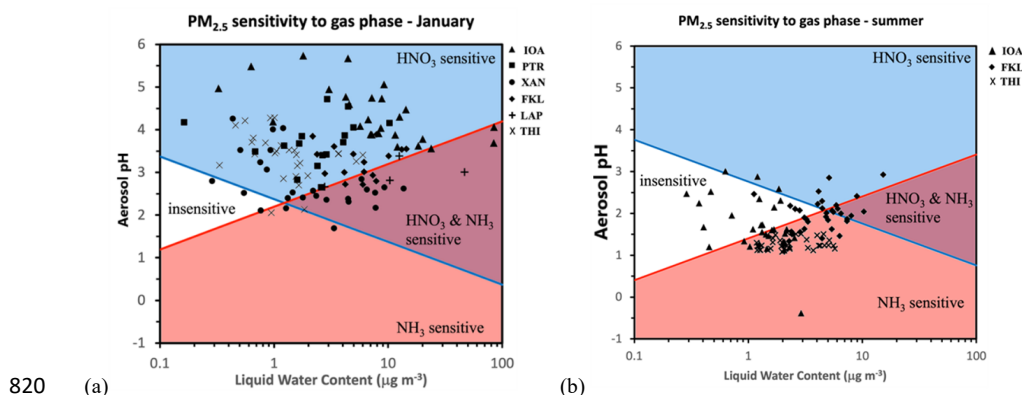


Figure 9: Chemical domains of sensitivity of  $PM_{2.5}$  mass to  $NH_3$  and  $NO_x$  emissions for the studied period (a) in winter (January) and (b) in summer (July and August). The average temperature used here is the mean measured one for the studied period at all sites in each season. Daily averaged values in each season of aerosol pH and liquid water content were used. The red line shows the characteristic aerosol pH as a function of liquid water content below which the  $PM_{2.5}$  mass is sensitive to  $NH_3$  levels and the blue line the characteristic aerosol pH as a function of liquid water content above which the  $PM_{2.5}$  mass is sensitive to  $HNO_3$  levels.

